Defects and Induced Densification in Neutron Irradiated Uranium Dioxide

1978

NOBUO NAKAE

)efects and Induced Densification in Neutron Irradiated Uranium Dioxide

1978

NOBUO NAKAE

CONTENTS

PREFACE

Most water-cooled reactors operate at present with oxide type fuels. Therefore, irradiation effects on uranium dioxide (UO_2) are important to operate nuclear reactors in safety. From this viewpoint, many works had been performed on UO_2 fuels. The works done up to 1961 were reviewed by J.Belle[1]. Although valuable results concerning with engineering standpoints of nuclear fuels were very aboundant, a basic study of irradiation effects on UO_2 has been scarce. Basic problems on UO_2 were pointed out in Geneva Conference held in 1964. Since then basic studies, for instance, dose dependence of physical properties (lattice parameter, thermal conductivity and electrical conductivity) and irradiation behavior of lattice defects in UO_2 have not been reported. Recently this kind of basic study has been initiated with respect to UC and UN in Germany[2]. In 1972, densification of fuel pellets during irradiation was observed in PWR. Furthermore, attention has been given to the pellet cladding mechanical interaction. In order to understand these phenomena, many works have been done in a half decade. In spite of much efforts, many problems remain unsolved at present.

In this study, at first, neutron irradiation effects on basic properties such as lattice parameter and density of UO_2 were investigated to get useful informations on interpreting the relation between the behavior of defects and irradiation induced densification. The fission dose dependence of these physical properties

including lattice strain, electrical conductivity and thermoelectric power was measured in the dose range from 1×10^{14} to 1×10^{19} fissions/cm^3. From the results of the measurements of lattice parameter, density and porosity, the concentrations of lattice defects such as interstitials and vacancies were estimated as a point defect. On the basis of these results a model for densification and an equation of the dose dependence of densification were proposed from kinetic consideration. The basic studies of irradiation effects on UO_2 yielded much help to better understanding not only of the densification but also of the diffusional problems such as the diffusion and the creep of irradiated UO_2 fuels.

This report consists of five chapters. In Chapt. 1, fission dose dependence of the lattice parameter and the lattice strain was described. The results of recovery annealings of lattice expansion were also shown. In the last part of this chapter, three kinds of kinetic equations, which were fitted well to experimental points, were mentioned with regard to the lattice parameter change. The effective volumes per fission event were also calculated by means of the equations.

In Chapt. 2, irradiation induced volume change was described accompanied with the results of density measurements. The volume change was discussed in connection with the lattice parameter change mentioned in Chapt. 1. From this discussion the behavior of irradiation produced various lattice defects was somewhat clarified.

In Chapt. 3, changes of electrical conductivity and thermoelectric power after neutron irradiation were described.

In Chapt. 4, concentrations of interstitials and vacancies produced during irradiation were estimated from the results of both lattice parameter and volume changes using the equations based on elastic continuum model of crystals. The vacancy concentration estimated here was applied to some diffusional properties of fuels under irradiation such as diffusion, densification and creep.

In the last chapter (Chapt. 5), availability of the densification model was shown in connection with the results obtained in the preceding chapters. Two problems were developed in this chapter, one of which was pore analysis and another the prediction of the dose dependence of the densification. A model for the densification was mentioned on the basis of the behavior of lattice defects, in particular vacancies.

References

[1] J. Belle (ed.), Uranium Dioxide: Properties and Nuclear Applications, (1961).

[2] W. Dienst, AECL-4375 (1973) and KFK-1215 (1970).

CHAPTER 1. FISSION DOSE DEPENDENCE OF LATTICE PARAMETER

1.1. Introduction

Only a few results are available on lattice defects in ceramic nuclear fuels such as uranium dioxide (UO_2), uranium carbides (UC, UC_2 and U_2C_3) and uranium mononitride (UN), though the knowledge about such lattice defects is indispensable to better understanding of irradiation behavior of fuel elements. Studies on dose dependence of lattice parameter change have been done by many investigators on carbides [1-10] and nitride [4,5,10], but those to UO_2 were scarce and only one work by Wait et al. [11-13] could be found in literatures. Most of these investigators had found that the lattice parameter increases as the fission dose and reaches a saturation value at a high fission dose. Some of them showed an abrupt decrease of the lattice parameter in a high dose range. In general, the curve representing the change of the lattice parameter in UO_2 vs. fission dose has a convex shape [11-13]. Dienst [4,5] had recently found a similar tendency in UC and UN. Matsui et al. [9] had also observed such a tendency in UC and found some difference caused by the difference of the surface area (sink density) between powered and massive specimens.

Formulations of a dose dependence of physical properties, such as lattice parameter and electrical resistivity, were tried by many workers [5,7,10,14]. They introduced almost similar

equations which predicted saturation with a single step or two steps to uranium metal, UC and UN.

In the present study, lattice parameter, lattice strain and recovery behavior have been investigated for irradiated UO_2 in order to understand the characteristics of fission induced lattice defects, and the results obtained here provide some interesting informations with respect to the UO_2 lattice defects. The concentration of these defects will be discussed in detail in other chapter (Chapt. 4). In this chapter, experimental data on the irradiation behavior of lattice defects was mainly described and the last part was dealt with the theoretical consideration in which dose dependence of the lattice parameter change was formulated and effective volume per fission event was estimated on the basis of the equations proposed here.

1.2. Experimetals

1.2.1. Specimens

Two sets of UO_2 pellets produced by sintering at 1700 °C in hydrogen atmosphere were commercially available and used in this experiment. The grain sizes were determined to be 2.5 and 5 μm by metallugical photographs. Impurity contents for the specimen of 5 μm grain size were listed in the mill sheet in table 1-1. Lattice parameters and densities before irradiation were measured to be 5.4707±0.0004 Å (94.50 %T.D.) and 5.4708±0.0004 Å (95.15 %T.D.), respectively, for the specimens of 5 and 2.5 μm grain sizes. One batch whose grain size was 2.5 μm had a O/U ratio of 2.002±0.005, whereas another batch, grain size of 5 μm, had a higher O/U of 2.004±0.0005. The O/U ratios were determined by a gravimetric method without correction of impurities. The lattice parameters indicate that the O/U ratios of both specimens are identical to 2.01 [15] . Some physical properties before irradiation are summarized in table 1-2.

1.2.2. Irradiations

Pellets were cut into segments (dimension of $\sim 1 \times 1 \times 10$ mm^3) by a diamond wheel slicing machine. The specimens sealed with quartz glass under a vacuum (about 10^{-3} torr) were put into a polyethylene or an aluminum capsule for irradiation. Irradiations were performed in HP, VG and VR holes in JRR-2 and

Table 1-1 Chemical analysis of impurity contents on UO_2 specimen of 5 μm grain size.

Element	Content (ppm)
Ag	< 0.2
Al	< 14
B	< 0.2
C	< 50
Ca	< 10
Cl	< 20
Cr	5
Cu	< 2
F	< 10
Fe	< 14
Mo	< 5
N	< 20
Ni	< 6
Si	< 6

Table 1-2 Physical properties before irradiation.

grain size (μm)	2.5	5
O/U ratio	2.002±0.005	2.004±0.0005
lattice parameter (Å)	5.4708±0.0004	5.4707±0.0004
density (%T.D.)	95.15±0.07	94.50±0.16

JRR-3 (JAERI). The characters of these irradiation holes were shown in table 1-3. Total fission doses were in a range between 1.14×10^{14} and 2.92×10^{18} fissions/cm^3. They were determined by the γ-activity of cobalt and/or cobalt-aluminum wire monitors placed in the quartz tube with the specimen. An estimated maximum specimen temperature during irradiation was below 150 °C, and this was confirmed by recovery experiments of lattice expansion mentioned after. Measurements of lattice parameter and lattice strain were carried out after cooling the irradiated specimens for two or three months.

1.2.3. Procedures

Lattice parameter of the specimens was measured using a double crystal X-ray diffractometer. Calculations of lattice parameters were carried out using eight peaks (333) to (444), and the errors were ±0.0004 Å.

The apparent lattice strain was calculated by the following relation : $\eta = \beta/\tan\theta$, where β is the increase or decrease of the X-ray peak half-width of irradiated UO_2 at the glancing angle θ of (333) as compared to that of pre-irradiation. This method was examined by Cullity [16] and Dienst [4] , who used the procedure similar to the above. Errors of η-values were ±10 %.

In order to examine the thermal recovery of lattice expansion, the irradiated specimens were annealed in purified argon atmosphere at an interval of 50 °C in the temperature range from 200 °C to

Table 1-3 Characters of HP, VG and VR positions.

irradiation hole	thermal neutron flux ($ncm^{-2}sec^{-1}$)
HP-1	1.7×10^{13}
HP-2	1.3×10^{13}
VG-7	2×10^{11} - 3.5×10^{12}
VR-1	2×10^{12} - 3.5×10^{13}
VR-3	2×10^{12} - 3×10^{13}

500 ^{o}C for one hour. The apparatus for recovery annealings was shown in fig.1-1. The lattice parameters were determined after cooling the specimens to room temperature.

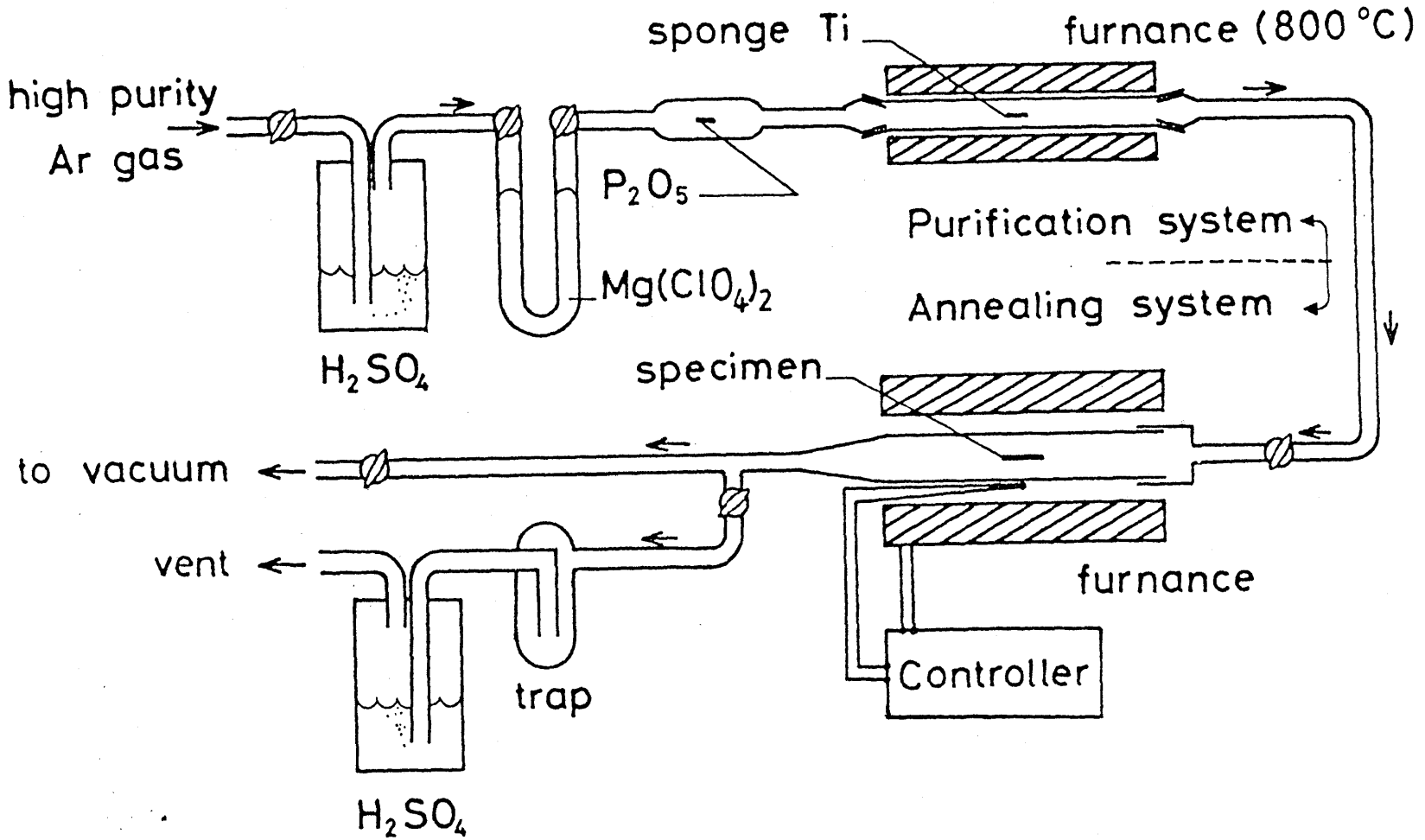

Fig.1-1. Apparatus for annealing experiments.

1.3. Results and discussion

1.3.1. Lattice parameter and lattice strain

Fig.1-2 shows variations of the lattice parameter and the apparent lattice strain of UO_2 as a function of the fission dose. Three definite stages, which were designated the first, the second and the third stage, respectively, in fig.1-2, appeared in the lattice parameter changes.

At the first stage, the lattice parameter increased with fission dose and was saturated up to 2.5×10^{16} fissions/cm^3 for 5 μm UO_2 and up to 2×10^{16} fissions/cm^3 for 2.5 μm UO_2. This type of saturation was not clearly observed in the results of single and polycrystalline UO_2 by Wait et al. [11-13]. On the other hand, a recovery of the apparent lattice strain was observed below 1×10^{15} fissions/cm^3. This behavior has not been observed in other ceramic fuels such as uranium carbide [4,5] and uranium nitride [4,5,17]. It is considered that the initial recovery is due to the relocation of excess oxygens frequently existing in the lattice matrix of UO_{2+x}. Furthere confirmation of this idea will be given by electrical resistivity measurements which will be mentioned in Chapt. 3. After that fission dose, the apparent lattice strain increased with fission dose in the first stage of the lattice parameter change.

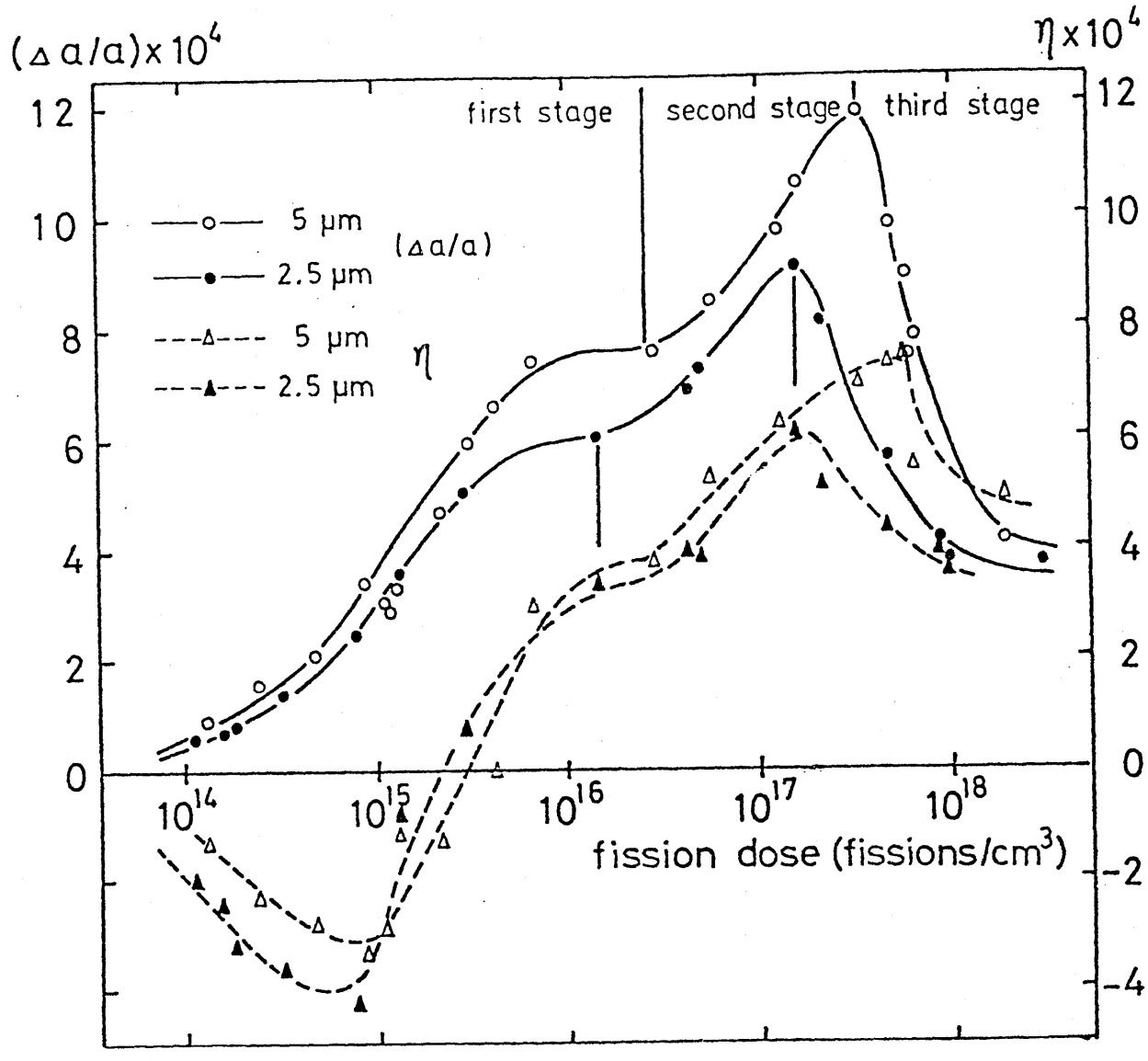

Fig.1-2. The variation of the lattice parameter and of the apparent lattice strain of UO_2 vs. the fission dose.

At the second stage, the lattice parameter increased again with fission dose, and reached a maximum at 3.2×10^{17} fissions/cm^3 for 5 μm UO_2 and at 1.6×10^{17} fissions/cm^3 for 2.5 μm UO_2. The second stage for the lattice strain change shifted to higher fission dose, compared with that for the lattice parameter change. This suggests that the concentration of vacancies is saturated after a maximum of concentration of interstitials.

At the third stage, the lattice parameter and the apparent lattice strain begin to decrease. This behavior can be explained in terms of kinetic considerations of defects described in the next section.

In our study, the lattice parameter changes for 2.5 μm UO_2 are smaller and are saturated earlier than those for 5 μm UO_2. This fact suggests that grain boundaries play an important role as sinks for knock-on atoms and interstitials. The maximum fractional change of the lattice parameter was 9.8×10^{-4} for single crystal UO_2 by Wait et al. [11], and this value was smaller than that for 5 μm UO_2, which was 11.86×10^{-4}. This might be explained by the difference in O/U ratio, because the specimens used by Wait et al. were stoichiometric and ours were hyper-stoichiometric. Stehle, Assmann and Wunderlich [18] investigated the effect of O/U ratio on Young's modulas in uranium oxide, and found that stoichiometric UO_2 had the maximum in Young's moduli. It is reasonably considered that irradiation-produced interstitials

can expand more easily the unit cell size in hyper-stoichiometric UO_2.

1.3.2. Annealing behavior of lattice parameter

The annealing behavior of the lattice parameter changes of 5 μm UO_2 irradiated to 1.28×10^{14}, 4.39×10^{14}, 4.28×10^{15}, 2.79×10^{16} (first stage), 1.54×10^{17}, 3.23×10^{17} (second stage) and 6.09×10^{17} fissions/cm^3 (third stage) is shown in figs.1-3 and 1-4. No recovery occurred below 150 °C in the sample irradiated to 1.28×10^{14} fissions/cm^3 (closed circles in fig.1-3).

The lattice expansion of UO_2 irradiated to 4.39×10^{14} fissions/cm^3 recovered completely at 250 °C. This suggests that simple types of defects are annealed out at 250 °C. Moreover the recovered lattice parameter is smaller than the original. This effect might be due to a dissociation of oxygen-interstitial-vacancy complexes [19] by irradiation. While two recovery steps were clearly observed between 150 and 250 °C and between 300 and 500 °C for the specimen irradiated to 2.79×10^{16} fissions/cm^3, which corresponded to the dose in the first saturation of the lattice parameter, and the defects produced were completely annealed out up to 500 °C. Primary defects produced in the first stage consist of two kinds of defects whose character is not clarified.

For the specimens irradiated to the second stage, two recovery

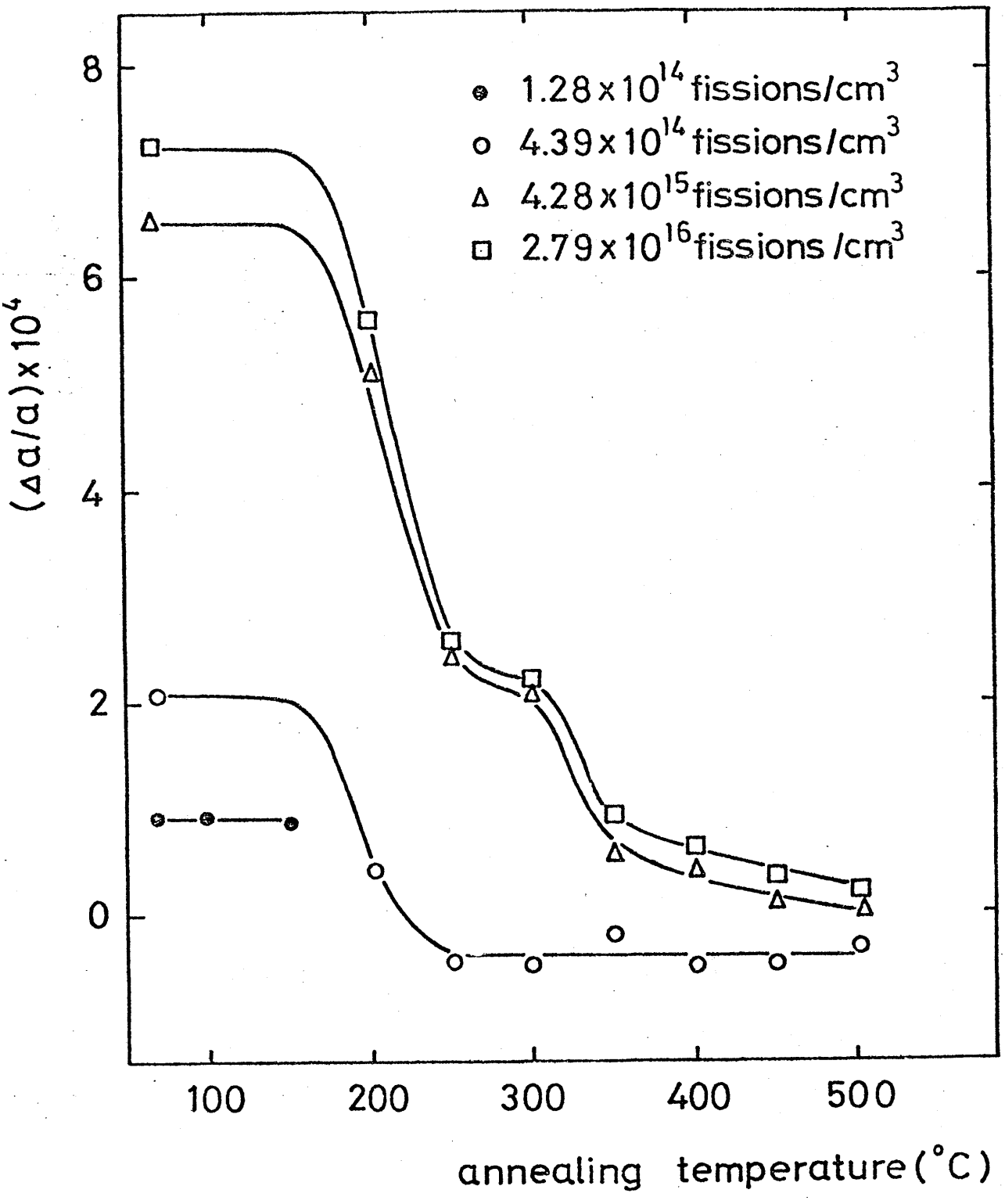

Fig.1-3. The annealing behavior of the lattice parameter changes of 5 μm UO_2 at the first stage.

steps were also observed at 200 (transition temperature) and 330 °C, although the second step was not clearly distinguished. Defects produced at this stage were not completely annealed out to 500 °C. There might have been interstitial clusters as observed with electron microscope by Whapham and Sheldon [20]. Recovery observations in situ by electron microscope are needed, and more precise experiments will clarify the nature of defects.

The result obtained for the specimen irradiated to the highest dose (the third stage in fig.1-2) was quite similar to that irradiated to the middle level (second stage), although a larger recovery was observed in the second step at 330 °C. The lattice expansion for the specimen irradiated to the highest dose was more completely recovered after annealing up to 500 °C than that irradiated in the second stage. This indicates that dominant defcets in the lattice in the latter specimen are more complex than those in the former.

Wait [21] observed two or three recovery steps in single crystal and polycrystalline UO_2, the first recovery step appeared at around 300 °C and the second seemed to appear above 500 °C. This suggests that excess uranium vacancies existing in hyper-stoichiometric UO_2 may play an important role on the recovery of the lattice expansion. The recovery curve obtained by Bloch [22] for single crystal UO_2 irradiated near 5×10^{17} fissions/cm^3 showed a trend similar to that obtained by Wait, but definite recovery steps were not reported.

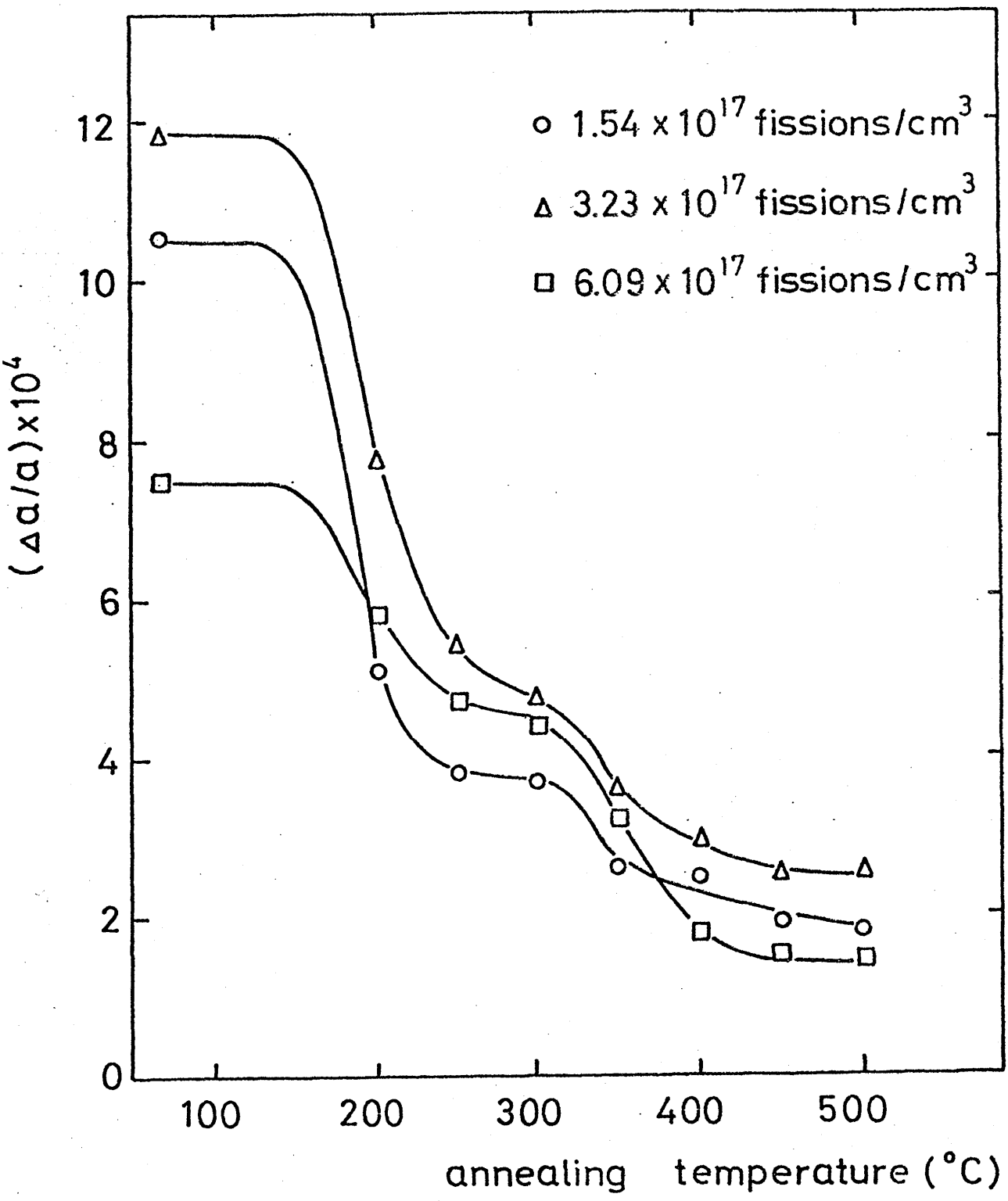

Fig.1-4. The annealing behavior of the lattice parameter changes of 5 μm UO_2 at the second and third stages.

1.4. Theoretical consideration

In this section kinetic considerations of lattice parameter changes with dose are described. Kinetic equations which predicted the relation between the lattice parameter changes and the fission dose were applied to dose dependence of lattice parameter changes not only to UO_2 but also to UC and UN.

1.4.1. Kinetic consideration for lattice parameter change under irradiation

The equations for the lattice parameter change under irradiation were deduced from kinetic considerations of the behavior of interstitials and vacancies. In the first stage, simple configurations of primary interstitials such as single- and di-interstitials saturate in the lattice at the experimental temperature. Thus the rate of the process will be described by a first order kinetic equation as follows:

$$dC_i/dt = V \Sigma_f \phi_{th}(1 - C_i),$$

where C_i is a fraction of interstitials to that at the saturation, $\Sigma_f \phi_{th}$ the fission density and V the volume effective for this process per fission event. Since it is reasonably assumed that the lattice parameter, a, is increased with the concentration of interstitials, the fractional increase of lattice parameter,

$\Delta a/\Delta a_1$, is proportional to C_i, provided that concentrations of vacancies are equal to or almost proportional to those of interstitials. Therefore, after the substitution $y = \Delta a/\Delta a_1$,

$$dy/dt = V_1 \Sigma_f \phi_{th}(1 - y),$$

where Δa_1 is the saturation value of Δa in the first stage. Then the usual equation is obtained;

$$\Delta a = \Delta a_1 \left\{1 - \exp(-V_1 \Sigma_f \phi_{th} t)\right\}. \qquad (1\text{-}1)$$

After the saturation of primary interstitials, rather complicated configurations of interstitials such as clustering in lattice matrix will be formed additionally, which will be called hereafter "secondary interstitials" as a whole. The production rate of these defects depends on both their concentration and that of residual atoms, provided that the velocities of annihilation by drift to sinks are proportional to the concentration of themselves. Therefore, the rate equation of the second order process is adopted for formation of the secondary interstitials. Substituting $y = \Delta a/\Delta a_2$,

$$dy/dt = V_2 \Sigma_f \phi_{th} y(1 - y), \qquad (1\text{-}2)$$

where Δa_2 is the saturation value of Δa in the second stage and

V_2 the effective volume for this process per fission. With the boundary condition that is $y = \Delta a_1 / \Delta a_2$ at $t = t_1$, the time of the first saturation, eq.(1-2) is solved:

$$\Delta a = \Delta a_2 \left[1 + \frac{\Delta a_2 - \Delta a_1}{\Delta a_1} \exp\left\{ -V_2 \Sigma_f \phi_{th} (t - t_1) \right\} \right]^{-1} . \qquad (1\text{-}3)$$

In the course of the above treatment, vacancies are apparently out of consideration, nevertheless they are included as follows. The relation between interstitials and vacancies was considered in the following manner. At low temperature only interstitials are expected to be mobile. A part of interstitials drifts to sinks such as grain boundaries , dislocations and fabricated pores, and others can annihilate with vacancies. As a result, the vacancy concentration becomes larger than that of interstitials in the lattice. As described in Chapt. 4 excess number of vacancies beyond interstitials in the lattice matrix is not so high compared with interstitials up to the end of the second stage. At the saturation of secondary interstitials mentioned before, all newly produced interstitials annihilate by above two processes. Therefore, even after the saturation, the vacancy concentration can increase without any change of the concentration of interstitials.

When the fission dose further increases, a number of excess vacancies are produced in the vicinity of the interstitials

existing at the second saturation. Then, these interstitials can easily annihilate with excess vacancies, while newly created interstitials cannot exist in the lattice because of a high enough concentration of vacancies. This kind of exhaustion of interstitials with excess vacancies begins when the concentration of excess vacancies in the lattice reaches a certain value, and proceeds to some extent until the concentration of excess vacancies saturates in the lattice. Therefore, with regard to the change of lattice parameter, the reduction of increased lattice parameter occurs and continues to the steady state provided that fission fragments do not give much influence. Hereafter this will be called the third stage. According to the above concept, the rate of decrease of lattice parameters in this stage is deduced in the following way. The rate of decrease of the concentration of interstitials is expressed with the equation:

$$-dC_i/dt = V_r \Sigma_f \phi_{th} C_{ir} C_{ex}, \qquad (1\text{-}4)$$

where C_i is the fractional concentration of interstitials relative to the saturation value at the end of the second stage and V_r is the effective volume for this process per fission. C_{ir} is the fractional concentration of interstitials recombinable with excess vacancies. When C_{i3} is the steady value of interstitials at the end of this stage, C_{ir} is expressed by,

$$C_{ir} = C_i - C_{i3}. \qquad (1\text{-}5)$$

On the other hand, C_{ex} is defined as the fractional concentration of excess vacancies effective to the exhaustion in this stage. According to the above concept, more than one excess vacancies, the number of which is defined as α, are needed to annihilate with one interstitial without any production of interstitials in this stage. It is assumed that one of these excess vacancies annihilates with an interstitial leaving surplus of excess vacancies in the lattice throughout this stage. Two cases are considered for C_{ex}, (1) concentration of vacancies corresponding to both interstitials, which have already annihilated, $(1 - C_i)$, and the stable interstitials at the end of this stage, C_{i3}, is C_{ex}, i.e.,

$$C_{ex} = \alpha(1 - C_i) + \alpha C_{i3} = \alpha(1 + C_{i3} - C_i), \qquad (1\text{-}6)$$

and (2) concentration of vacancies corresponding to only to $(1 - C_i)$ is C_{ex}, i.e.,

$$C_{ex} = \alpha(1 - C_i). \qquad (1\text{-}7)$$

Eq.(1-6) is based on the assumption that C_{ex} is the concentration of vacancies corresponding to interstitials except recombinable ones, which remain without annihilation, $(1 - C_{ir})$, and in this case, the same equation as eq.(1-6) is obtained as follows:

$$C_{ex} = \alpha(1 - C_{ir}) = \alpha\{1 - (C_i + C_{i3})\} = \alpha(1 + C_{i3} - C_i).$$

As mentioned later, the former concept predicts the experimental data better than the latter one. According to the former concept, the following relation can be obtained from eq.(1-6);

$$C_{ex2} = \alpha C_{i3}, \tag{1-8}$$

where C_{ex2} is the concentration of excess vacancies at the end of the second saturation. Consequently, eq.(1-6) means that C_{ex} involved excess vacancies produced in this stage and also excess vacancies existing at the second saturation. Substituting eq.(1-5) and eq.(1-6) to eq.(1-4),

$$-dC_i/dt = \alpha V_r \Sigma_f \phi_{th}(C_i - C_{i3})(1 + C_{i3} - C_i). \tag{1-9}$$

Since $\Delta a/\Delta a_2 = y$ is proportional to C_i and $\Delta a_3/\Delta a_2 = y_3$ to C_{i3}, eq.(1-9) corresponds to

$$-dy/dt = V_3 \Sigma_f \phi_{th}(y - y_3)(1 + y_3 - y), \tag{1-10}$$

where V_3 is the effective volume for this process per fission. Integrating eq.(1-10) with the boundary condition that $y = 1$ at $t = t_2$,

$$\Delta a = \Delta a_2 \frac{(\Delta a_2 - \Delta a_3)\exp\{-V_3 \Sigma_f \phi_{th}(t - t_2)\}}{\Delta a_3 + (\Delta a_2 - \Delta a_3)\exp\{-V_3 \Sigma_f \phi_{th}(t - t_2)\}} + \Delta a_3, \tag{1-11}$$

where Δa_2 and Δa_3 are the saturation values at the second and the third stage, respectively.

1.4.2. Application of the kinetic consideration to experimental data

The three equations, (1-1), (1-3) and (1-11), were applied to UO_2 in the present study and other works.

The effective volumes of V_1, V_2 and V_3 were obtained by substituting the present results into these equations, and were summarized in table 1-4 together with other constants of Δa_1, Δa_2, Δa_3, $\Sigma_f \phi_{th} t_1$ and $\Sigma_f \phi_{th} t_2$. The curves illustrated in fig.1-2 are obtained by fitting eqs.(1-1), (1-3) and (1-9) to the experimental data.

The changes of lattice parameters of UC and UN with dose in the first and second stages calculated from the data by Adam and Rogers [1,10] and Bloch [3] were compared with the curves calculated with their single stage equation. As shown in fig.1-5, the curves calculated by these equations fit the data well. The least square values of V_1 and V_2 are compared with the V given by each author in table 1-5. The data of powdered UC by Matsui [9] were analyzed as the second and the third stages, and arc melted UC by Matsui [9] was analyzed for all stages. The data of UC by Childs [6,7] were analyzed as the second stage and powdered UC

Table 1-4 Effective volumes in each stage for the specimens of 2.5 and 5 μm grain sizes, and other constants of Δa_1, Δa_2, Δa_3, $\Sigma_f \phi_{th} t_1$ and $\Sigma_f \phi_{th} t_2$. Effective volumes were obtained by means of eqs.(1-1), (1-3) and (1-11) with other constants.

	$V_1(cm^3)$	$V_2(cm^3)$	$V_3(cm^3)$	Δa_1	Δa_2	Δa_3	$\Sigma_f \phi_{th} t_1$	$\Sigma_f \phi_{th} t_2$
UO_2(5μm)	6.44×10^{-16}	1.16×10^{-17}	4.59×10^{-18}	7.40×10^{-4}	11.8×10^{-4}	4.00×10^{-4}	2.50×10^{16}	3.23×10^{17}
UO_2(2.5μm)	6.68×10^{-16}	2.58×10^{-17}	5.59×10^{-18}	6.00×10^{-4}	9.10×10^{-4}	3.60×10^{-4}	2.00×10^{16}	1.55×10^{17}

$\Sigma_f \phi_{th} t$: fissions/cm^3

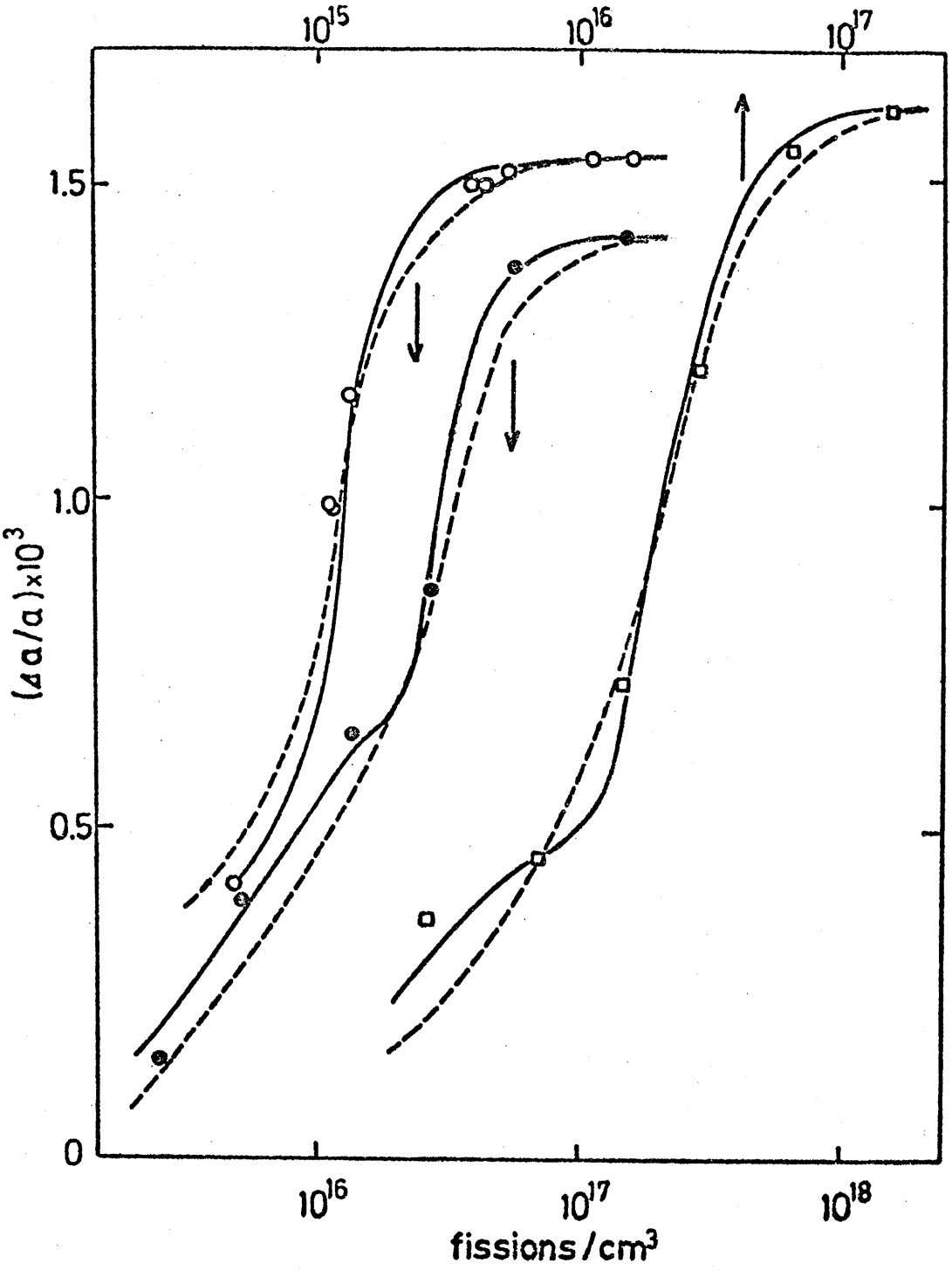

Fig.1-5. Comparison of analysis of the first order kinetics with that of the second order. Dotted lines and solid lines indicate the forst and the second order, respectively. ○ : UC [3], ● : UC [1,10], □ : UN [1,10]. Circles correspond to the lower abscissa and squares to the upper abscissa.

Table 1-5 Effective volumes of lattice parameter change per fission event.

Specimen	V_1-value (cm^3)	V_2-value (cm^3)	V-value (cm^3)	Remarks
UC [3]		$(1.57\pm0.34)\times10^{-16}$	8.20×10^{-17}	sintered pellet
UC [1,10]	$(1.42\pm0.50)\times10^{-16}$	$(7.49\pm1.18)\times10^{-17}$	3.96×10^{-17}	powder
UN [1,10]	$(3.54\pm0.72)\times10^{-16}$	$(1.12\pm0.13)\times10^{-16}$	4.83×10^{-17}	powder

by Dienst [4,5] was analyzed as the second and the third stages. The calculated curves for these data are represented in fig.1-6. In this figure, reliable data for UO_2 by Wait were also illustrated with the calculated curves. The curve with a dot-dash-line for arc-melted UC in the third stage was less reliable because the irradiation temperature was higher than that for low doses [23]. The least square values of V_1, V_2 and V_3 in the above data are indicated in tables 1-5 and 1-6.

1.4.3. Discussion

Comparing the specimens of 5 μm grain size with those of 2.5 μm grain size, the saturation doses for both the first and the second stages are low in the latter, and their saturation values of Δa are lower than those of the former. Similar trends were observed between single and polycrystals UO_2 by Wait et al. and between the platelet and the powdered UC by Matsui. It is reasonably explained from the fact that the specimens with smaller grain size have larger sink densities for interstitials at surfaces and/or grain boundaries than those with bigger grain size. In comparison of the effective volumes in the same stages, the volume becomes larger with an increase of sink densities as indicated in the results obtained for UO_2 of this author, UC of Matsui and UO_2 of Wait et al.. This suggests that the effective volume of each stage depends on the sink densities. The relation between the volume and the sink densities is described

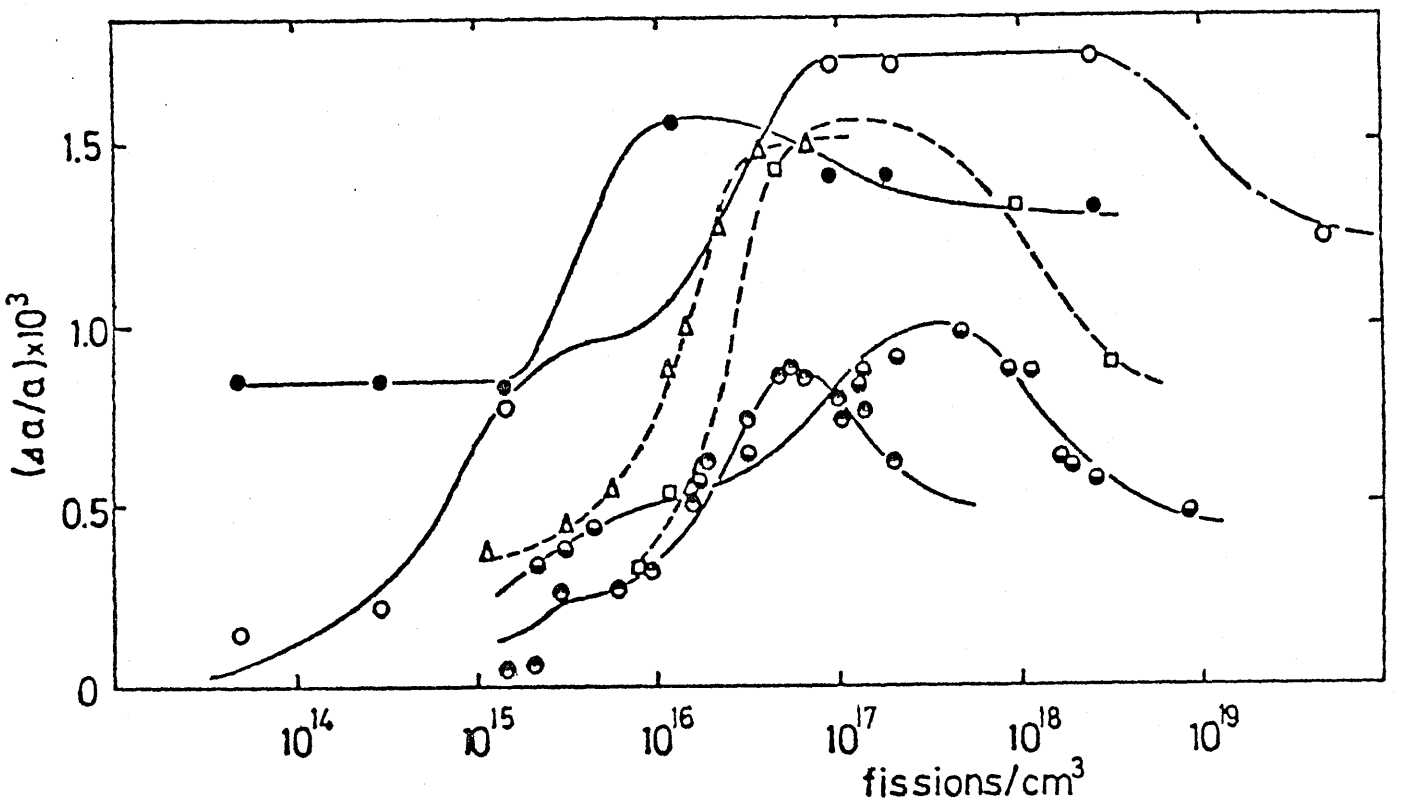

Fig.1-6. Lattice parameter change with fission dose for UC and UO_2.
● : hypo-UC powdered [9], o : hypo-UC platelet [9], □ : UC [4,5], Δ : UC [6,7], ⊖ : UO_2 single crystal [11-13], ⊖ : UO_2 polycrystal [11-13]. Solid and dotted lines indicate the calculated curves. The dot-dash-line is less reliable.

Table 1-6 Effective volumes of lattice parameter change per fission event.

Specimen	V_1-value (cm^3)	V_2-value (cm^3)	V_3-value (cm^3)	Remarks
UC [9]	$(8.49\pm0.86)\times10^{-16}$	3.53×10^{-17}	1.24×10^{-19}	plate arc melted, hypostoichiometry
UC [9]		4.98×10^{-16}	$(1.19\pm0.17)\times10^{-17}$	powder arc melted, hypostoichiometry
UC [4,5]		1.03×10^{-16}	8.28×10^{-19}	powder
UC [6,7]		$(1.33\pm0.01)\times10^{-16}$		arc melted
UO_2 [11-13]	$(2.92\pm0.09)\times10^{-16}$	$(1.98\pm0.61)\times10^{-17}$	$(1.22\pm0.13)\times10^{-18}$	single crystal
			$(5.69\pm3.81)\times10^{-18}$	calculated by eq.(1-12)
UO_2 [11-13]	$(5.11\pm3.64)\times10^{-16}$	$(7.86\pm1.54)\times10^{-17}$	$(1.29\pm0.24)\times10^{-17}$	polycrystal
			$(4.93\pm3.00)\times10^{-17}$	calculated by eq.(1-12)

in Appendix 1.1.

Dienst [5] treated the third stage with the first order reaction and gave 2×10^{-18} cm^3 for the effective volume (to which he called vacancy core overlapping volume) on UC and UO_2. Since in this stage reaction proceeds between interstitials and vacancies, it should be treated with the second order. Various concepts can be made for the second order rate process between residual interstitials and vacancies. In addition to eq.(1-10), the following equations were examined using the data obtained here and by others [5,6,9,12]. Most of data give the best precision to the value of the effective volumes by eq.(1-10):

$$-dy/dt = V_3 \Sigma_f \phi_{th}(y - y_3)(1 - y), \qquad (1\text{-}12)$$

$$-dy/dt = V_3 \Sigma_f \phi_{th}(y - y_3)y, \qquad (1\text{-}13)$$

$$-dy/dt = V_3 \Sigma_f \phi_{th}(y - y_3)^2. \qquad (1\text{-}14)$$

In above equations, eq.(1-12) can be easily considered because the terms, $(y - y_3)$ and $(1 - y)$, respectively, are proportional to the concentration of recombinable interstitials and of excess vacancies produced after the second saturation of interstitials. However, the precision was not good for all the data except UC by Dienst, and, as an example, standard deviation of V_3 calculated from eq.(1-12) for UO_2 by Wait et al. are represented in table 1-6.

The following model can be proposed for the third stage.

(1) Except for the case where $\Delta a_3 = 0$, excess vacancies relative to interstitials are present in the end of the second stage.

(2) Moreover, excess vacancies are additively produced in the third stage due to drift of interstitials to sinks, and some of those produced are used up to recombination with residual interstitials.

(3) It becomes clear that the reduction of lattice parameter in the third stage begins after the concentration of excess vacancies reaches a certain value and the attainment depends on the velocity of drift of interstitials to sinks. This is the reason for the difference in observed saturation values for specimens prepared from the same materials.

References

[1] J. Adam and M. D. Rogers, Reactor Sci. Tech. 14 (1961) 151.

[2] M. J. Bloch and C. Marchix, CEA 202 (1961).

[3] M. J. Bloch and J. P. Mustelier, J. Nucl. Mater. 17 (1965) 350.

[4] W. Dienst and D. Brucklacher, Proc. Int. Symp. Ceramic Nuclear Fuels, Amer. Ceram. Soc. (1969) p82.

[5] W. Dienst, KFK-1215 (1970) and AECL-4375 (1973).

[6] B. G. Childs, A. Ogilvie, J. C. Ruckman and J. L. Whitton, "Radiation Damage in Reactor Materials", IAEA (1963) p241.

[7] B. G. Childs, J. C. Ruckman and K. Buxton, "Carbide in Nuclear Energy, vol.2", Macmillan (1964) p849.

[8] H. Matsui, T. Kirihara and T. Ohmichi, J. Nucl. Sci Tech. 9 (1972) 618.

[9] H. Matsui, J. Nucl. Mater. 56 (1975) 161.

[10] M. D. Rogers and J. Adam, AERE-R 4046 (1962).

[11] E. Wait, M. J. Duck, A. C. Fox, E. E. Jackson and A. R. Junkins "Radiation Damage in Solids, vol.2", IAEA (1962) p231.

[12] L. E. Roberts, P. Brook, J. R. Findlay, B. R. Frost, L. E. Russell, J. B. Sayers and E. Wait, 3rd UN Int. Conf., P/155 Geneva (1964).

[13] E. Wait, cited in L. Leteurtre and Y. Quéré (ed.), "Defects in Fissile Materials", North-Holland Publ. Co., Amsterdam, (1972) p75.

[14] Y. Quéré, cited in R. Strumane, J. Nihoul, R. Gevers and S. Amelinckx (ed.), "The Interaction of Radiation with Solids", North-Holland Publ. Co., Amsterdam, (1963) p346.

[15] J. Belle (ed.), Uranium Dioxide: Properties and Nuclear Applications, (1961) p174.

[16] B. D. Cullity, "Elements of X-ray Diffraction", Addison-Wesley Publ. Co., Inc., Reading, Massachusetts, U.S.A..

[17] M. Tamaki, private communication.

[18] H. Stehle, H. Assmann and F. Wunderlich, Advanced Course on In-reactor Behavior of Water Reactor Fuels and Its Influence on Design, Manufacture and Operation, organized by Netherlands-Norwegian Reactor School at Institutt for Atomenergi, Norway, (1974).

[19] H. M. Lee, J. Nucl. Mater. 56 (1975) 81.

[20] A. D. Whapham and B. E. Sheldon, Phil. Mag. 12 (1965) 1179.

[21] E. Wait, cited in B. T. Bradbury and B. R. T. Frost, "Radiation Effects in Ceramic Fuels, in Dienes, Studies in Radiation Effects, vol.2", Gordon and Breach, New York (1967) p180.

[22] M. J. Bloch, J. Nucl. Mater. 3 (1961) 237.

[23] H. Matsui, private communication.

Appendix 1.1. Relation between the effective volume and the sink density

In this appendix, overlapping volume of the first stage is considered in connection with the relation between the effective volume and the sink density.

In N_K knock-on atoms, N_A atoms annihilate with vacancies spontaneously and N_I atoms are formed as Frenkel defects and end up in interstitial positions and N_S atoms migrate to sinks such as grain boundaries and dislocations per fission. Then, the following relation is given,

$$N_K = N_A + N_S + N_I, \qquad (A.1\text{-}1)$$

i.e.,

$$1 = N_A/N_K + N_S/N_K + N_I/N_K = \alpha + \beta + \gamma, \qquad (A.1\text{-}2)$$

where α, β and γ represent the fractions of N_A, N_S and N_I to N_K. Now we introduce a concept of collosion numbers, and $N(E_0)$ and $N(E_I)$ are defined as the collision numbers for producing a knock-on atom and an interstitial atom, respectively. Since it is assumed that total collision number per fission (N_{col}) is constant, the following relation can be obtained,

$$N_K N(E_0) = N_I N(E_I) = N_{col}$$

i.e.,

$$N(E_I) = \frac{N_K N(E_0)}{N_I} = N(E_0)/\gamma. \qquad (A.1\text{-}3)$$

In the first stage, the rate of increase of interstitials depends on the number of uncolloding atoms. Then, the following rate equation is given,

$$dN_I/dt = \frac{\Sigma_f \phi_{th}}{N_0} N_I^{s1} N(E_I) - \frac{\Sigma_f \phi_{th}}{N_0} N_I N(E_I),$$

$$= \Sigma_f \phi_{th} \frac{N(E_I)}{N_0} N_I^{s1}\left(1 - \frac{N_I}{N_I^{s1}}\right), \qquad (A.1\text{-}4)$$

where N_0 is the number of atoms in unit volume and N_I^{s1} is the number of interstitials at the first saturation.
Substituting eq.(A.1-3) to eq.(A.1-4), eq.(A.1-4) is rewritten by the equation;

$$dN_I/dt = \Sigma_f \phi_{th} \frac{N(E_0)}{N_0 \gamma} N_I^{s1}\left(1 - \frac{N_I}{N_I^{s1}}\right). \qquad (A.1\text{-}5)$$

In eq.(A.1-5) we can defined

$$V_1 = \frac{N(E_0)}{N_0 \gamma} \quad ,$$

as an effective volume for an interstitial atom. And the above equation is rewritten as follows using eq.(A.1-2),

$$V_1 = \frac{N(E_0)}{N_0(1 - \alpha - \beta)} . \qquad \text{(A.1-6)}$$

In eq.(A.1-6) $N(E_0)/N_0$ is constant for a given material, and in addition, the value of $(1 - \alpha)$ is constant at a given irradiation temperature. Consequently, eq.(A.1-6) indicates that the effective volume, V_1, becomes small with increasing β value, i.e., sink density. The difference of V_1 values between 2.5 μm and 5 μm grain sizes specimens can be easily explained on the basis of the above consideration.

CHAPTER 2. IRRADIATION INDUCED VOLUME CHANGE IN UO_2

2.1. Introduction

In order to get informations about the irradiation behavior of lattice defects, the measurements of bulk density and porosity were done in this chapter. Recently, density changes of uranium dioxide after irradiation had been studied by many workers [1-6] at high doses (more than 1×10^{20} fissions/cm^3). At lower doses (up to 1×10^{18} fissions/cm^3), however, less studies were reported; Kingery et al. [7,8] measured the density changes at only two doses of 8.6×10^{15} and 8.3×10^{16} fissions/cm^3, and they reported that the density decrease at lower dose corresponded to the expected value from the lattice parameter measurements by Wait et al. [9], while at higher dose it exceeded the value expected from the lattice parameter. Kingery et al. assumed that the excess density change at the higher dose was due to interstitial clusters. Porosity changes had been investigated by many workers [4,5,6], and porosity decreases were observed in high dose range above 1×10^{19} fissions/cm^3.

In the present study, bulk density changes in UO_2 were measured from 1.14×10^{14} to 2.92×10^{18} fissions/cm^3. The bulk density decreased in the dose range up to 5.6×10^{16} fissions/cm^3, and above this dose an abrupt increase (i.e., densification) was observed. Porosity changes were also measured in the higher dose range where the bulk density increased. The decrease of

porosity was observed above 2×10^{17} fissions/cm^3. The bulk volume and pore volume changes were calculated using these results and the mechanism of irradiation-induced volume change was discussed on the basis of irradiation behavior of lattice defects.
The results of lattice parameter measurements in Chapt. 1 were also referred in this chapter. The concentrations of lattice defects such as interstitials and vacancies estimated from the measured lattice parameter, density and porosity will be shown in the chapter 4.

2.2. Experimental

2.2.1. Specimens and irradiations

Irradiated UO_2 specimens used in the density and the porosity measurements were the same as those used in the lattice parameter measurements. Therefore, the description of specimens and irradiation procedure was omitted in this chapter.

2.2.2. Procedures

Several methods for density measurements were reported by many workers [4,10,11,12]. In this study, the densities were measured using the m-xylene immersion method with a spring balance made of quartz as shown in fig.2-1; the sensitivity of the spring balance is 0.212 mm/mg. Densities before and after irradiation were determined using the following equation:

$$d = \rho (l_{0A} - l_A)/(l_{0L} - l_L), \qquad (2\text{-}1)$$

where d and ρ are the densities of the specimen and m-xylene, respectively, and l_{0A} and l_0 are readings of the spring balance length with the basket only and after loading a specimen in air, and l_{0L} and l_L are the corresponding readings in liquid, respectively. Measurements for each specimen were carried out five times and the errors were ± 0.1 %. The fractional bulk volume

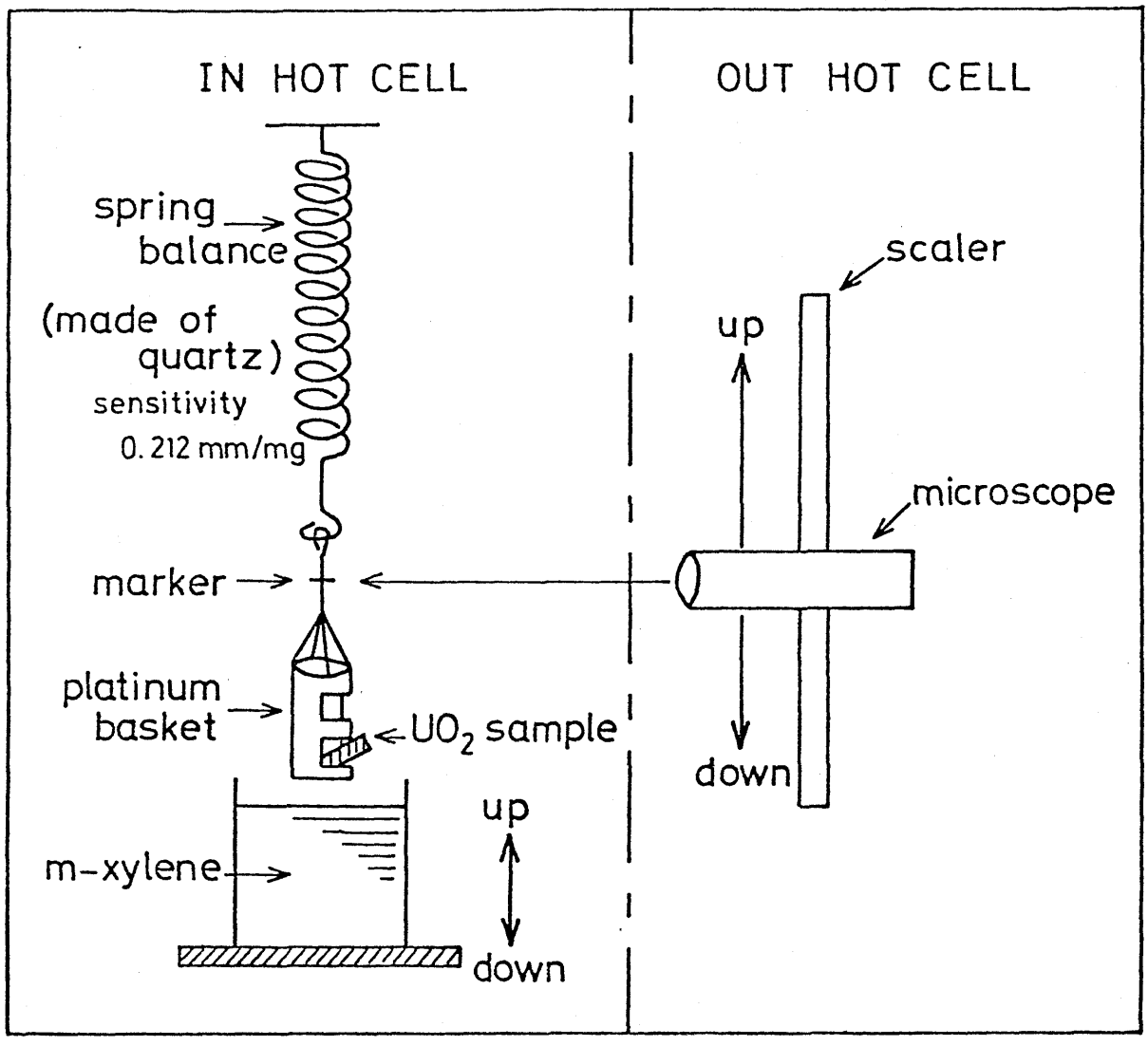

Fig.2-1. Schematic diagram of the apparatus for density measurements.

change, $\Delta V_d/V$, was calculated from the data of density changes using the relation:

$$\Delta V_d/V = (d_0 - d)/d, \qquad (2\text{-}2)$$

where d_0 and d are the pre- and post-irradiation densities.

The porosity measurements were carried out using a QTM-720 type image analyser. Metallography is an only direct means of studying pore shrinkage. The irradiated samples were polished carefully to avoid rounding or filling of the pores with grinding debris. The samples were examined in the as-polished state. Photomicrographs were taken and analyzed using a QTM-720 type image analyser (an automated television microscope system) to determine the distribution of pores by size classes and the volume of porosity. By comparing with the pre-irradiation pore volume the amount of pore removal can be determined. The fractional pore volume change, $\Delta V_p/V$, was calculated from the data of porosity changes as follows:

$$\frac{\Delta V_p}{V} = \frac{P(V + \Delta V_d) - P_0 V}{V} = (P - P_0) + P(\Delta V_d/V), \qquad (2\text{-}3)$$

where P_0 and P are the pre- and post-irradiation porosities.

2.3. Results

2.3.1. Density change after irradiation

The densities after irradiation are tabulated in table 2-1 and the fractional changes are shown in fig.2-2 together with those obtained by Kingery et al. [7,8] . Densities decrease with dose up to 5.6×10^{16} fissions/cm^3, and the corresponding fractional decreases are almost the same for both specimens of 2.5 and 5 μm grain sizes. A steep increase of densities (i.e., densification) follows above 5.6×10^{16} fissions/cm^3, and the densities are getting to the original values at about 6×10^{17} fissions/cm^3 for the specimen of 5 μm grain size and at about 5×10^{17} fissions/cm^3 for the specimen of 2.5 μm grain size. Above these doses the densification of the specimen with smaller grain size proceeds faster than that with larger grain size. The density change obtained by Kingery et al. up to 8.3×10^{16} fissions/cm^3 gave smaller values than ours, probably because their specimen was stoichiometric UO_2 with large grain size.

2.3.2. Porosity change after irradiation

The porosities after irradiation are tabulated in table 2-2. Only the result is used to calculate the pore volume changes in this chapter. The result will be discussed in detail in the last chapter.

able 2-1 The densities after neutron irradiation in both specimens of 2.5 and 5 μm grain sizes.

2.5 μm		5 μm	
$\Sigma_f \phi_{th} t$ (fissions/cm^3)	density (g/cm^3)	$\Sigma_f \phi_{th} t$ (fissions/cm^3)	density (g/cm^3)
re-irradiation	10.419±0.008	pre-irradiation	10.349±0.017
$.14\times10^{14}$	10.417±0.010	1.28×10^{14}	10.343±0.015
$.59\times10^{14}$	10.417±0.009	2.35×10^{14}	10.342±0.015
$.79\times10^{14}$	10.412±0.006	4.39×10^{14}	10.337±0.007
$.29\times10^{14}$	10.411±0.022	1.10×10^{15}	10.329±0.007
$.78\times10^{14}$	10.400±0.008	1.20×10^{15}	10.322±0.011
$.28\times10^{15}$	10.390±0.002	2.20×10^{15}	10.315±0.006
$.95\times10^{15}$	10.377±0.010	4.28×10^{15}	10.300±0.009
$.45\times10^{16}$	10.307±0.007	6.81×10^{15}	10.247±0.013
$.27\times10^{16}$	10.249±0.015	2.42×10^{16}	10.224±0.006
$.92\times10^{16}$	10.241±0.005	2.79×10^{16}	10.202±0.010
$.52\times10^{17}$	10.307±0.005	5.58×10^{16}	10.169±0.012
$.12\times10^{17}$	10.362±0.003	1.24×10^{17}	10.200±0.011
$.79\times10^{17}$	10.404±0.009	1.54×10^{17}	10.217±0.010
$.48\times10^{17}$	10.550±0.004	3.23×10^{17}	10.282±0.012
$.97\times10^{17}$	10.544±0.008	4.63×10^{17}	10.301±0.007
$.92\times10^{18}$	10.603±0.009	5.68×10^{17}	10.332±0.012
		6.12×10^{17}	10.383±0.011
		1.90×10^{18}	10.467±0.008

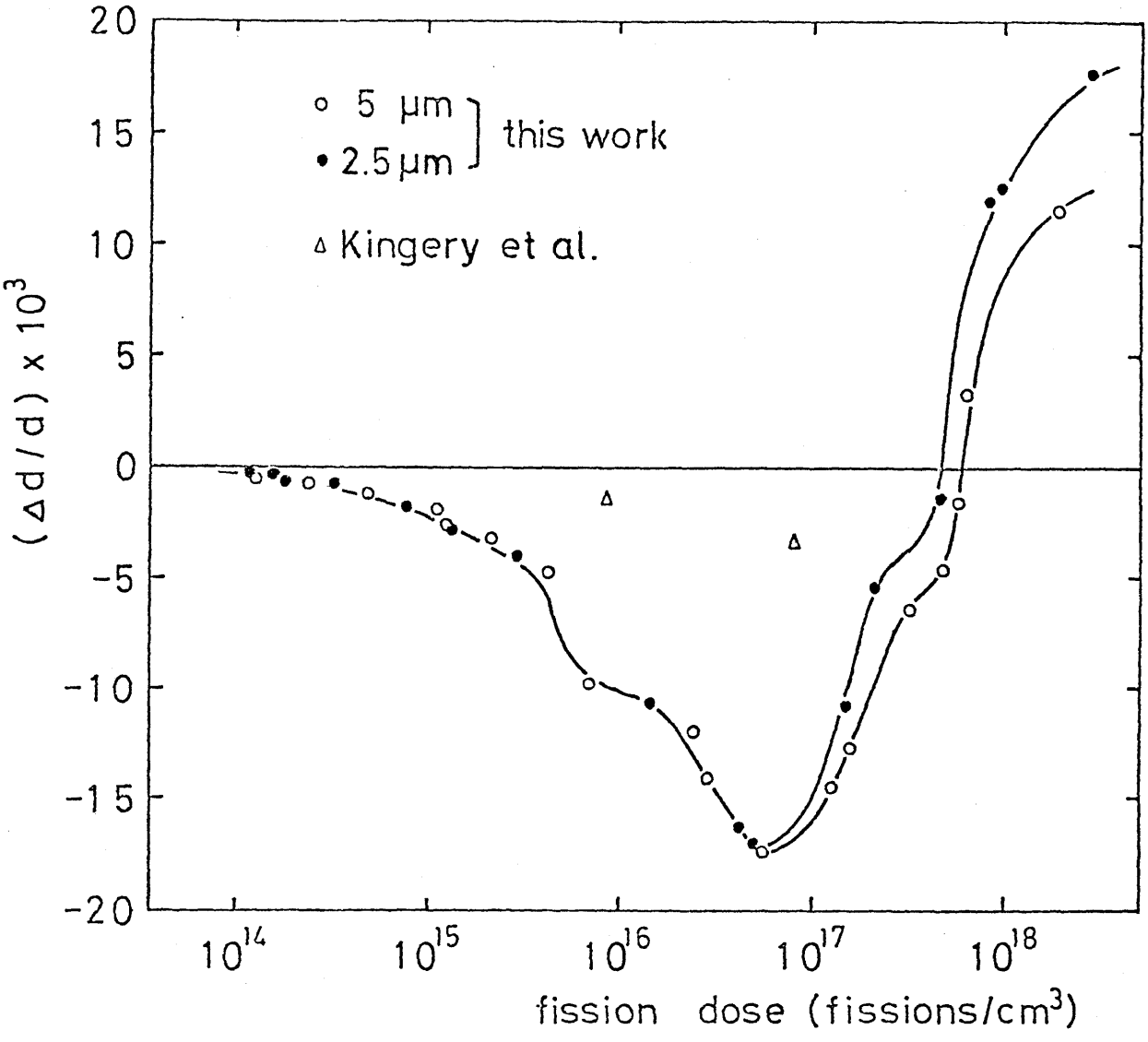

Fig.2-2. Fractional changes of density in UO_2 after neutron irradiation.

Table 2-2 The porosities after neutron irradiation in both specimens of 2.5 and 5 μm grain sizes.

2.5 μm		5 μm	
$\Sigma_f \phi_{th} t$ (fissions/cm^3)	porosity (%)	$\Sigma_f \phi_{th} t$ (fissions/cm^3)	porosity (%)
pre-irradiation	4.8±0.2	pre-irradiation	5.5±0.2
2.12×10^{17}	4.0	4.63×10^{17}	4.6
2.92×10^{18}	3.1	1.90×10^{18}	4.0

2.4. Discussion

The fractional bulk volume changes are calculated by eq.(2-2) and are shown in fig.2-3 as a function of dose together with the values of $3(\Delta a/a)$. There are four stages of bulk volume change in the dose range between 1.1×10^{14} and 2.9×10^{18} fissions/cm^3 as shown in this figure. The bulk volume increases in first two stages, and then it decreases in the last two stages.

In the first stage, the values of $\Delta V_d/V$ almost correspond to or are slightly larger than $3(\Delta a/a)$. If interstitials and vacancies are equal in number, the following relation is satisfied for the macroscopic volume change of crystals without porosity:

$$\Delta V_d/V = 3(\Delta a/a). \qquad (2\text{-}4)$$

Therefore, in the first stage interstitials and vacancies are produced in equal number, or some of the displaced atoms diffuse to sinks such as dislocations and grain boundaries. In the latter case the atom migrating to sinks forms a Schottky type defect which represents an isolated vacancy in one of the two sublattices with an adatom at a sink or at the surface. Consequently, the vacancy concentration is expected to increase faster than that of interstitials. This phenomena depend on the fact that the migration energy of interstitials is lower than that of vacancies. The migration energies of uranium interstitial

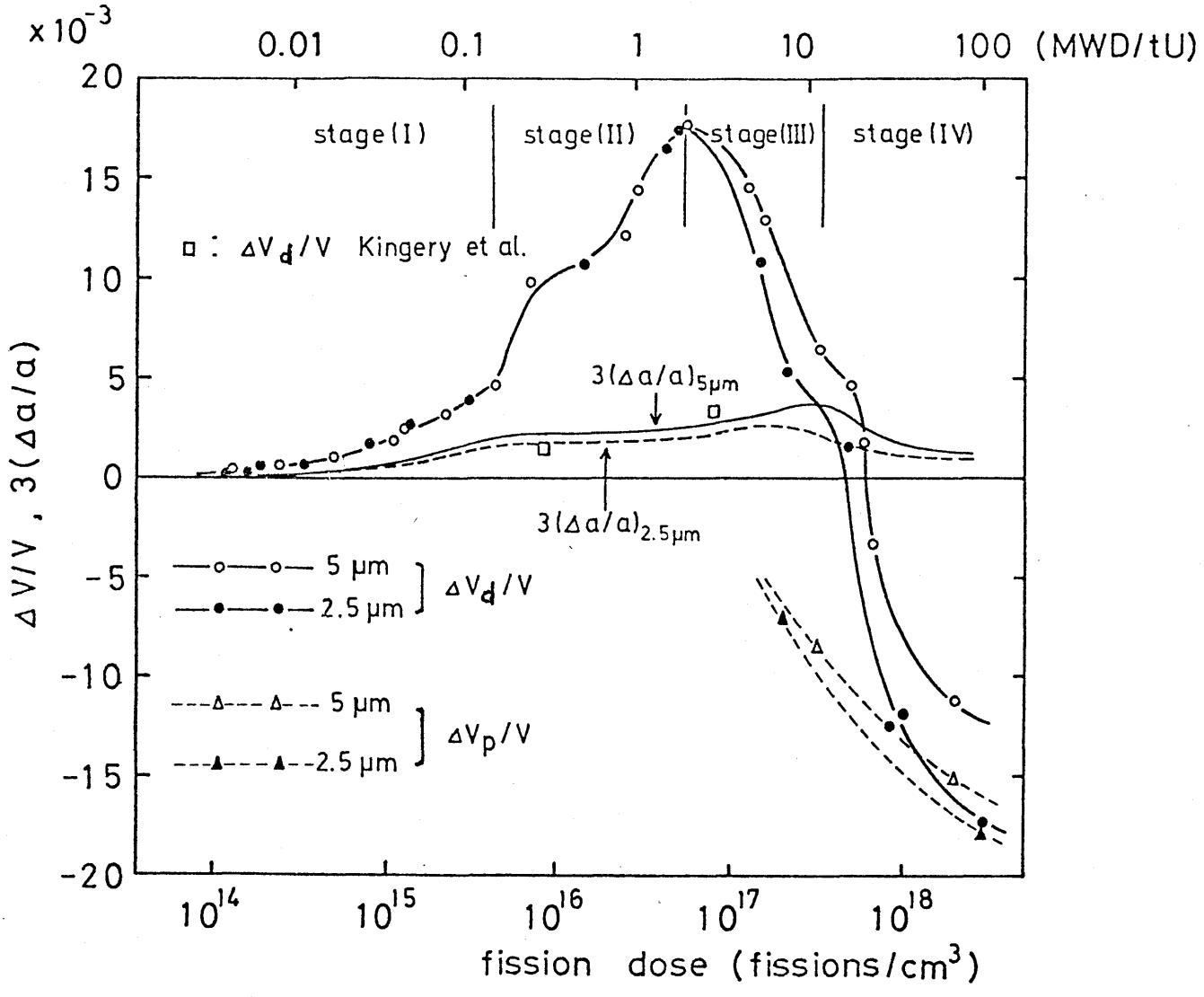

Fig.2-3. Fractional bulk volume changes, $\Delta V_d/V$, of UO_2 which were calculated by means of eq.(2-2) using the results of bulk density measurements and fractional pore volume changes, $\Delta V_p/V$, which were calculated by eq.(2-3).

and vacancy in UO_2 obtained from literatures [13-15] are shown in table 2-3.

In the second stage, $\Delta V_d/V$ grately exceeds $3(\Delta a/a)$. This means that a large number of Schottky type defects are produced. Grain boundaries, dislocations and clusters were considered as sinks for displaced atoms, which yielded a volume increase. The detailed explanation for it will be made in the chapter 4. Considering the observation of Whapham and Sheldon [16], who reported clusters of interstitials in UO_2 at a dose of 4.3×10^{15} fissions/cm^3 with an electron microscope, we presumed that interstitial clustering might play an important role on the large volume increase in this stage. The increase of lattice parameters in the second stage where the secondary interstitials are produced is observed after the rapid increase of bulk volume. From this fact we speculate that the secondary interstitials are produced after interstitial clustering. But more electron microscope observation will be needed. Fission product gas atoms gave no effects to this large bulk volume increase of $\Delta V_d/V = 1.77$ % at a dose of 5.6×10^{16} fissions/cm^3, because their concentration was very small and their mobility is negligible at the low irradiation temperatures used here. It should be noticed that the dose at which the maximum bulk volume increase was observed corresponded the reported dose for maximum elongation of stack length of UO_2 fuel elements in the starting period of BWR [17].

Table 2-3 The migration energies of uranium interstitial and vacancy in UO_2.

interstitial (eV)	vacancy (eV)	reference
0.3	2.2	[13]
	2.4±0.4	[14]
1.5~1.7	~2.4	[15]

The fractional pore volume changes calculated by eq.(2-3) are also shown in fig.2-3. In the third and fourth stages, the bulk volume decreases and also the pore volume decreases. However, there are differences between $\Delta V_d/V$ and $\Delta V_p/V$ as shown in this figure. The differences, which are due to defects and defect clusters as mentioned in the chapter 4, tend to become small with increasing dose, indicating that defects and defect clusters annihilate with vacancies. The value of $\Delta V_p/V$ is close to that of $\Delta V_d/V$ for the specimen of 2.5 μm grain size irradiated to 2.9×10^{18} fissions/cm^3. This shows that annihilation of defects and defect clusters in the smaller grain size specimen almost ends at this dose. On the other hand, some defects and defect clusters are left in the larger grain size specimen. Therefore, two mechanisms, (1). annihilation of defects and defect clusters and (2). pore shrinkage, should be considered for the bulk volume decrease (i.e., densification). The decrease of bulk volume occurs after that of lattice parameter in higher dose range. From the fact, it is considered that interstitial clusters existing outside of the lattice matrix are less stable than interstitials in the lattice matrix. This speculation might be supported by the electron microscope observation of Whapham and Sheldon [16], who reported the annihilation of interstitial clusters in higher dose range.

References

[1] A. Hanevik and P. Arnesen, HIR-066 (1973).

[2] H. M. Ferrari, E. Roberts and J. Scott, Paper 54, British Nuclear Energy Society Symposium on Nuclear Fuel Performance, London, UK (1973).

[3] I. J. Hastings, D. H. Rose and M. H. Schankula, J. Amer. Ceram. Soc. 58 (1974) 74.

[4] D. A. Banks, J. Nucl. Mater. 54 (1974) 97.

[5] W. Chubb, A. C. Hott, B. M. Argall and G. R. Kilp, Nucl. Tech. 26 (1975) 486.

[6] M. Uchida, K. Yanagisawa and M. Ichikawa, JAERI-M-6904 (1977).

[7] W. D. Kingery, Y. Kauffmann, M. Bruet and B. de Bernardy, CEA-R 3289 (1967).

[8] W. D. Kingery, Y. Kauffmann, M. Bruet and B. de Bernardy, J. Nucl. Mater. 26 (1968) 204.

[9] E. Wait, M. I. Duck, A. C. Fox, E. E. Jackson and A. R. Junkinson, in "Radiation Damage in Reactor Materials", Proc. Symp., IAEA (1963) p241.

[10] K. S. B. Rose, J. Williams and G. Potts, J. Nucl. Mater. 51 (1974) 195.

[11] A. F. Reid, A. H. Halff, Science, 135 (1962) 319.

[12] A. S. Roy, Anal. Chem. 33 (1961) 1426.

[13] S. R. MacEwen and I. J. Hastings, Phil. Mag. 31 (1975) 135.

[14] Hj. Matzke, AECL-2585 (1966).

[15] Hj. Matzke, Proc. Int. Conf. Plutonium 1975 and other actinides North-Holland Publ. Co., Amsterdam, (1976) p801.

[16] A. D. Whapham and B. E. Sheldon, Phil. Mag. 11 (1965) 1179.
[17] Y. Niki, et al., THE HITACHI HYORON, 58 (1976) 81.

CHAPTER 3. ELECTRICAL CONDUCTIVITY AND THERMOELECTRIC POWER CHANGES IN IRRADIATED UO_{2+x}

3.1. Introduction

The electrical properties of UO_2 have been studied by several investigators. Two reviews have been written by Meyer [1] for the work up to 1940 and Willardson and Moody [2] for the work up to 1961. UO_2 is a p-type extrinsic semi-conductor below 800 °C and the positive holes due to deviations from the stoichiometric composition contribute to its conductivity. Above 800 °C it is transformed into intrinsic. Willardson et al. [3] interpreted the conductivity on the assumption that UO_2 was an usual semi-conductor and that a band picture was valid. It was shown, however, by Heikes and Johnston [4] that band theory was inadequate, and they explained the conduction mechanism by a jumping of electrons (or holes) from one cation to a neighoring one. Aronson et al. [5] used the ideas of Heikes and Johnston in order to explain the electronic conduction in UO_2. They assumed an activated jumping of localized holes between U^{5+} and U^{4+} in UO_{2+x} and introduced the concept of the hopping mechanism of conduction in UO_2. They also showed that the electrical conductivity in the single phase region could be represented by

$$\sigma \simeq 2x(1 - 2x)\exp(-\Delta E/RT), \qquad (3\text{-}1)$$

and also for thermoelectric power, Q,

$$Q = (k/e)\ln(1 - 2x/2x), \qquad (3\text{-}2)$$

where x corresponds to the excess oxygen in UO_{2+x}.
Recently, Lee [6] proposed that in the extrinsic region oxygen interstitial-vacancy complexes which existed in hyper stoichiometric UO_2 contributed to the conductivity in UO_{2+x}.

Studies of radiation damage on electrical properties are scarce. The influence of fission fragment damage on the electrical conductivity of UO_2 single crystals of stoichiometric and hyper stoichiometric compositions has been studied by Nagels et al. [7]. They observed an appreciable decrease of conductivity in hyper stoichiometric UO_2 sample up to about 4×10^{15} fissions/cm^3, and a constant value appeared after that dose, suggesting a saturation of damage in UO_2. The electrical conductivity of stoichiometric sample remained practically unchanged after exposures up to 1.6×10^{16} fissions/cm^3. The fact that the conductivity of the hyper stoichiometric samples decreased markedly showed that the defect centres produced by irradiation acted trapping sites to holes, and the initial free hole concentration was reduced.
On the other hand, Roake [8] found that an abrupt increase in the conductivity occurred at 1.56×10^{19} fissions/cm^3 and he proposed that the increase was due to a change of conduction mechanism from the p-type to the n-type.

Thermoelectric power measurements were performed by Aronson et al. [5] and Wolfe [9] for non-irradiated hyper

stoichiometric UO_2 at various temperatures. These authors pointed out that the conduction mechanism at lower temperatures differed from that at higher temperatures, and in higher temperature UO_2 crystals were transformed into intrinsic semi-conductors.

In the present study, the fission dose dependences of both electrical conductivity and thermoelectric power were investigated for the specimens irradiated in the dose range from 1×10^{15} to 2×10^{18} fissions/cm^3, and the results were discussed in terms of irradiation induced lattice defects.

3.2. Experimental

3.2.1. Specimens and irradiations

Irradiated specimens used for electrical property measurements are the same as those for the lattice parameter measurements. The details of the specimens and irradiation procedures are shown in Chapt. 1 (section 1.2.1 and 1.2.2). Electrical conductivity and thermoelectric power for non-irradiated specimens are summarized in table 3-1.

3.2.2. Apparatus

Electrical resistivity measurements were carried out using the dc four-probes (needles) potential-drop method at room temperature. The electrical resistivity was calculated by a following equation:

$$\rho_0 = 2\pi S\{F_2^2(1/S)F_3^2(1/S)/G_6(W/S)\}V/I. \qquad (3\text{-}3)$$

In eq.(3-3), correction for shape of the specimens was taken into account, where F_2, F_3 and G_6 are the correction factors which are functions of 1/S and W/S, where W is thickness of the specimen, l distance between needle and boundary of the specimen, and S spacing between adjacent needles. ρ_0 is specific resistivity, V potential drop between two needles, and I supplied current. Corrections for porosity were made with the following equation [10].

Table 3-1 Electrical conductivity and thermoelectric power of both specimens of 2.5 and 5 μm grain sizes before irradiation.

	2.5 μm	5 μm
E.C.	$(8.03\pm0.05)\times10^{-5}\ \Omega^{-1}cm^{-1}$	$(9.43\pm0.12)\times10^{-4}\ \Omega^{-1}cm^{-1}$
T.E.P.	0.71 ± 0.07 mV/deg	0.95 ± 0.09 mV/deg

$$\rho = \rho_0/\{1 + P/(1 - P^{2/3})\}, \qquad (3\text{-}4)$$

where ρ_0 is specific resistivity calculated by eq.(3-3), ρ the actual resistivity and P the volume fraction of pores, (i.e., the porosity which is calculated from the results of bulk density measurements obtained in Chapt. 2). The error is less than ± 2 %.

The apparatus of thermoelectric power measurements is shown in fig.3-1. A temperature gradient of 5-6 °C was obtained by an external cooling system (one side of the specimens was cooled by copper held at 0 °C). In order to measure the temperature differences differential chromel-alumel thermocuples was used. The potential differences between two potential leads were measured with a vibrating reed electrometer. The measurements were carried out at around room temperature. The error was less than ± 10 %.

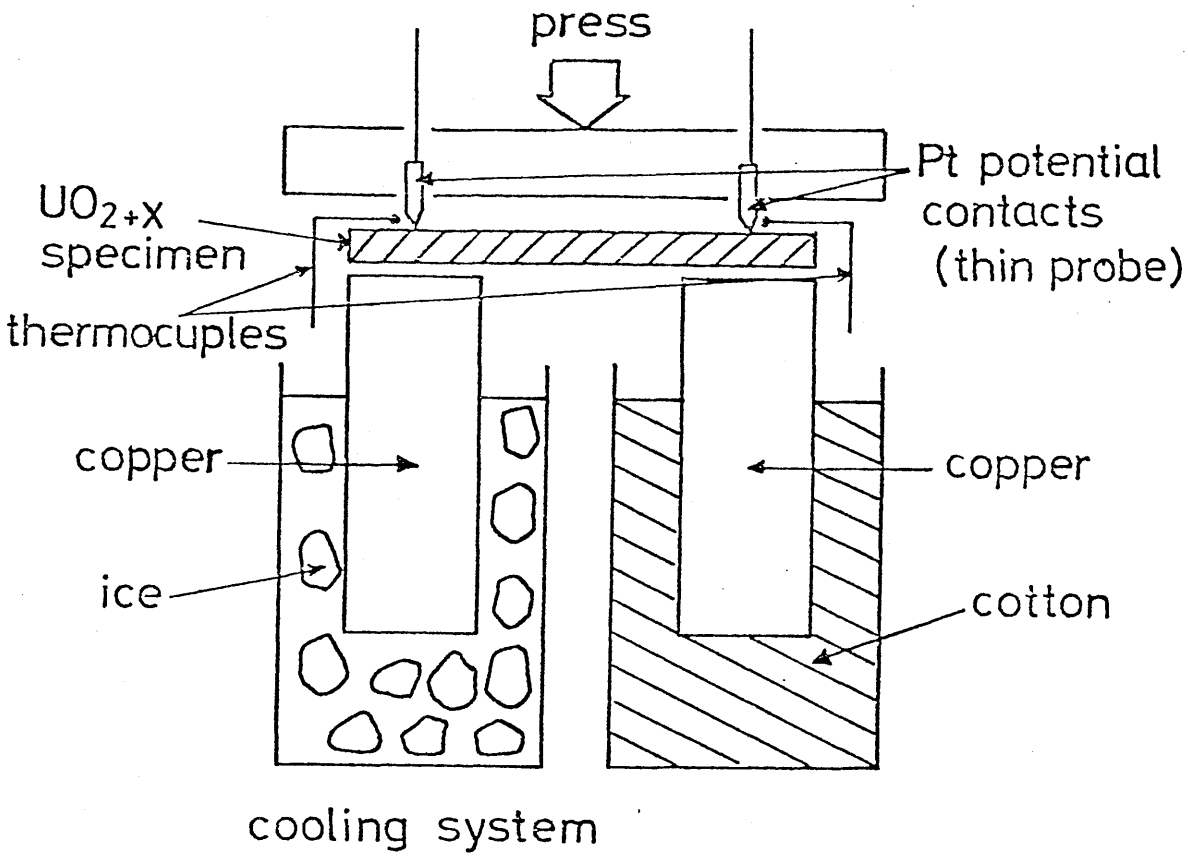

Fig.3-1. Schematic diagram of the apparatus for thermoelectric power measurement.

3.3. Results

As shown in table 3-1, one order of difference in conductivity was observed in the two different UO_2 specimens. Though many investigators [5,9,11,12] found that conductivity increased with increase of x in UO_{2+x}, the conductivity was also sensitively affected by grain size, lattice strain and impurities. For example, Wolfe [9] reported that the difference in relative mean grain diameters of 60 and 150 μm UO_2 might account for higher conductivity of the latter. From the thermoelectric power measurements it was calculated that the x-values in UO_{2+x} for specimen A (2.5 μm) and B (5 μm) were 5.20×10^{-6} and 3.92×10^{-6}, respectively by use of eq.(3-2). These values are much smaller than those expected from the lattice parameters and by the gravimetric method (see section 1.2.1), possibly because thermoelectric power is also affected by impurities. The discrepancy of O/U ratios doesn't matter in the context of this chapter, because this paper deals mainly with the dose dependence of electrical properties.

Electrical conductivity and thermoelectric power for the irradiated UO_2 are tabulated in table 3-2 and table 3-3, and illustrated in fig.3-2. A steep decrease in conductivity is observed for both specimens in the dose range up to 1×10^{15} fissions/cm^3, corresponding to the previously reported decrease of lattice strain observed at the beginning of irradiation (see section 1.3.1). After that the conductivities of both specimens are almost identical and gradually increase in the dose

Table 3-2 Electrical conductivity and thermoelectric power after irradiation for the specimen of 5 μm grain size.

$\Sigma_f \phi_{th} t$ (fissions/cm^3)	E.C. (Ω^{-1}cm^{-1})	T.E.P. (mV/deg)
1.28×10^{14}	$(1.23\pm0.11)\times10^{-4}$	
2.35×10^{14}	$(1.12\pm0.05)\times10^{-5}$	
4.39×10^{14}	$(6.41\pm0.28)\times10^{-6}$	
1.20×10^{15}	$(3.42\pm0.18)\times10^{-6}$	0.45 ± 0.04
2.20×10^{15}	$(3.52\pm0.19)\times10^{-6}$	
4.28×10^{15}	$(3.68\pm0.18)\times10^{-6}$	
6.81×10^{15}		0.50 ± 0.05
2.79×10^{16}	$(3.93\pm0.22)\times10^{-6}$	
5.58×10^{16}	$(4.41\pm0.25)\times10^{-6}$	
1.54×10^{17}	$(4.49\pm0.22)\times10^{-6}$	
3.23×10^{17}	$(5.07\pm0.21)\times10^{-6}$	
4.63×10^{17}	$(4.01\pm0.22)\times10^{-6}$	
5.68×10^{17}	$(4.68\pm0.28)\times10^{-6}$	
6.12×10^{17}	$(4.75\pm0.27)\times10^{-6}$	0.42 ± 0.04
1.90×10^{18}	$(9.62\pm0.55)\times10^{-6}$	0.15 ± 0.01

Table 3-3 Electrical conductivity and thermoelectric power after irradiation for the specimen of 2.5 μm grain size.

$\Sigma_f \phi_{th} t$ (fissions/cm^3)	E.C. (Ω^{-1}cm^{-1})	T.E.P. (mV/deg)
1.59×10^{14}	$(6.58\pm0.13)\times10^{-6}$	0.63 ± 0.06
3.29×10^{14}	$(5.86\pm0.14)\times10^{-6}$	
7.78×10^{14}	$(4.79\pm0.09)\times10^{-6}$	
1.28×10^{15}	$(3.19\pm0.03)\times10^{-6}$	
2.59×10^{15}		0.44 ± 0.04
4.27×10^{16}	$(4.66\pm0.11)\times10^{-6}$	0.45 ± 0.04
1.52×10^{17}	$(4.71\pm0.06)\times10^{-6}$	0.55 ± 0.06
4.79×10^{17}	$(5.74\pm0.12)\times10^{-6}$	
9.97×10^{17}	$(4.51\pm0.07)\times10^{-6}$	0.38 ± 0.04

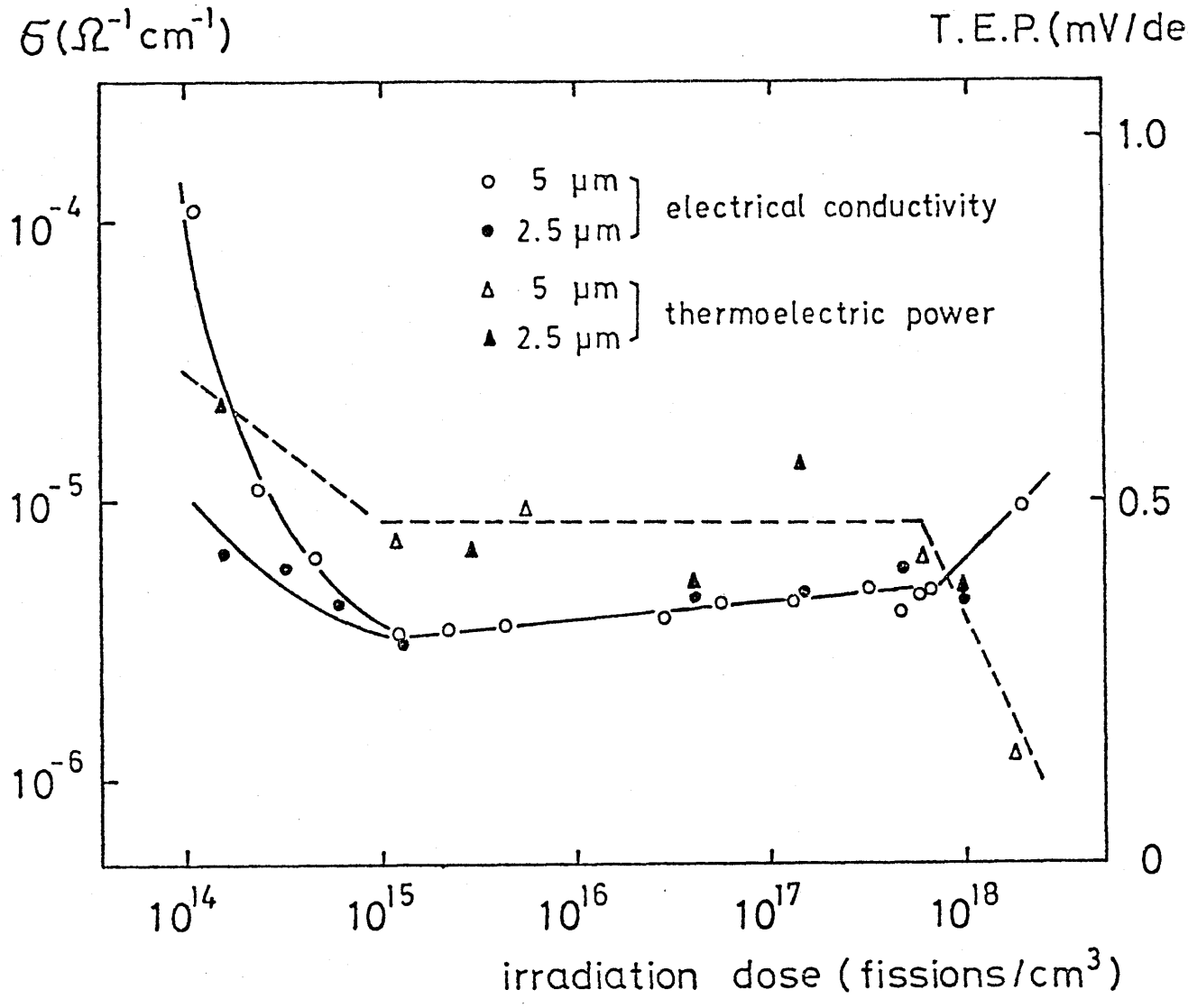

Fig.3-2. Changes of electrical conductivity and thermoelectric power in UO_{2+x} after neutron irradiation.

range between 1×10^{15} and 1×10^{18} fissions/cm^3. An abrupt increase of conductivity is observed in the specimen B at higher dose (more than 1×10^{18} fissions/cm^3). The conductivity for the specimen A at higher dose could not be measured because the specimen A accidentally broken after irradiation.

The thermoelectric power change in both specimens after irradiation shows a similar behavior. It decreases with increasing dose up to 1×10^{15} fissions/cm^3, and then remains constant in the dose range between 1×10^{15} and 6×10^{17} fissions/cm^3. A steep decrease occurs abruptly above 6×10^{17} fissions/cm^3 in specimen B. A positive sign of thermoelectric power (0.153 ± 0.01 mV/deg at a dose of 1.90×10^{18} fissions/cm^3) obtained here indicates that the p-type conduction mechanism contributes to the electrical conductivity.

3.4. Discussion

The electrical properties of UO_2 without irradiation have been studied by several investigators, and it is well known that single-phase UO_{2+x} without any precipitation of U_4O_9 is a p-type extrinsic semi-conductor. The conductivity of such UO_{2+x} arises from the positive holes due to deviation from stoichiometry. Aronson et al. [5] proposed the conduction mechanism in UO_{2+x} in terms of an activated jumping of localized holes between U^{5+} and U^{4+} in UO_{2+x}, and thus introduced the concept of hopping mechanism to UO_{2+x}.

The initial decrease of conductivity in irradiated UO_2 has been studied by Nagels et al. [7] and the results of them are shown in fig.3-3. They explained the decrease in conductivity as a trapping of holes with defect centres by irradiation. They found that the conductivity was saturated at 4×10^{15} fissions/cm and explained this saturation in terms of overlapping of fission tracks. According to their consideration, the fraction of volume affected by the fission track, taking into account overlapping, was given by the formula:

$$f_{vol} = 1 - e^{-V_0 N}, \qquad (3\text{-}5)$$

where N is the number of tracks per cm^3 and V_0 the volume of a track. Introducing $V_0 = 4.5\times10^{-16}$ ($d = 100$ Å, $l = 6$ μm), one found that 97 % of the volume was affected by fission tracks

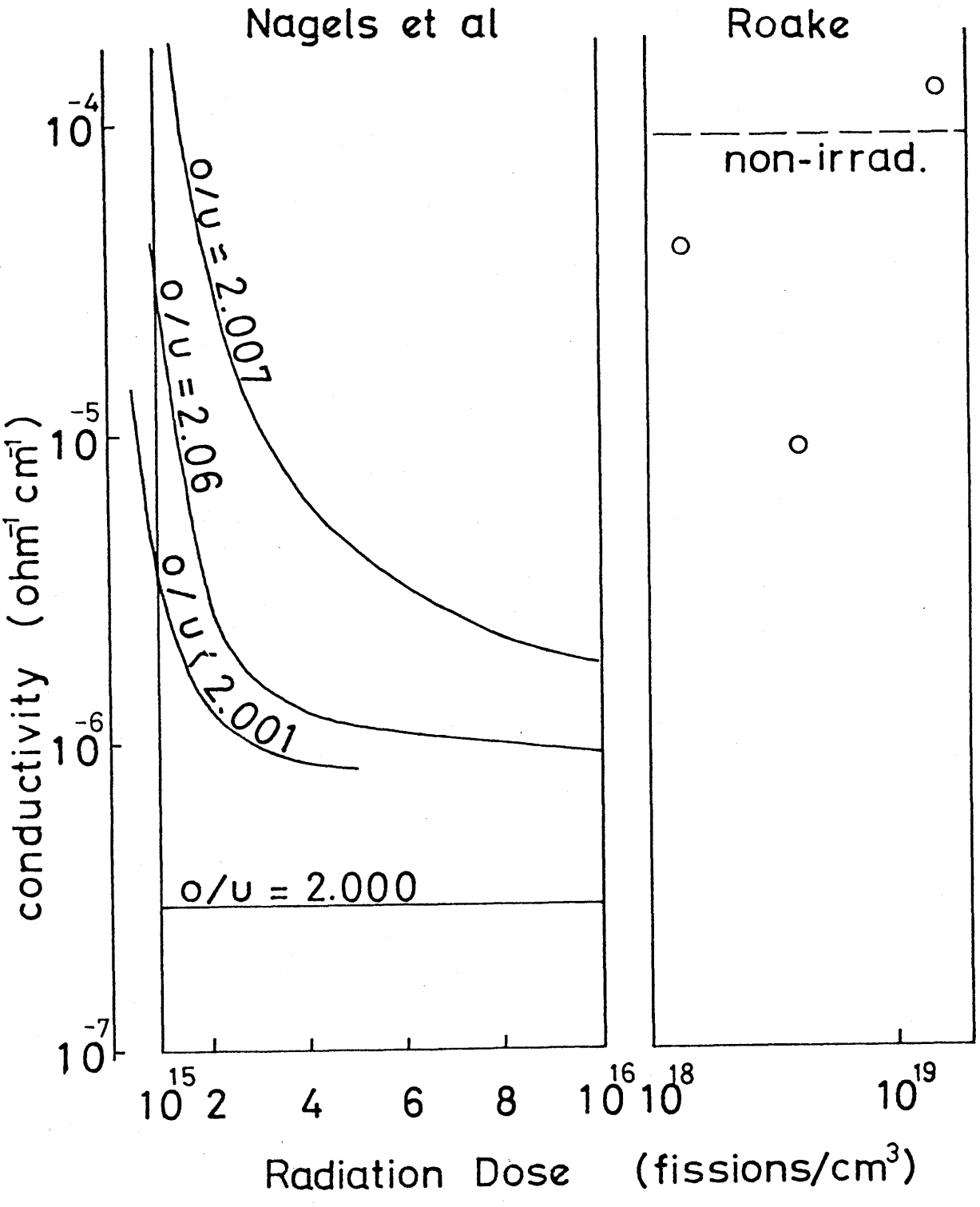

Fig.3-3. Results of electrical conductivity in UO_2 after neutron irradiation by Nagels et al. [7] and Roake [8].

for $N = 8\times10^{15}$ /cm^3 (or 4×10^{15} fissions/cm^3), and 100 % for $N = 10^{16}$/cm^3. There was a good agreement between the experimentally observed and the calculated value of the number of fission tracks at which saturation of damage occurred. In our measurement, however, the saturation of electrical conductivity is not clearly observed at this dose, and the conductivity gradually increases after the initial decrease. The explanation by Nagels et al. is, therefore, not adequate to explain our results.

Lee [6,13] investigated the following two conduction mechanisms:

$$U^{5+}(5f) + O^{2-}(2p^6) = U^{4+}(5f^2) + O^{-}(2p^5) \qquad E_1 = 0.78 \text{ eV} \qquad (3\text{-}6)$$

$$(O_i' O_v O_i'') - U^{5+}(5f) + O^{2-}(2p^6) = (O_i' O_v O_i'') - U^{4+}(5f^2) + O^{-}(2p^5)$$

$$E_2 = 0.32 \text{ eV} \qquad (3\text{-}7)$$

where $(O_i' O_v O_i'')$ is an oxygen interstitial-vacancy complex, which is similar to Willis complex [14], and E_1 and E_2 are energy differences between both sides of eqs.(3-6) and (3-7).
He concluded that the oxygen interstitial-vacancy complexes associated with U^{5+} ions could play an important role on fast transport of holes. Because the activation energy of conduction in p-type extrinsic region is comparable to E_2. During irradiation the complexes might be decomposed (thus causing the decrease of hole mobility).

On the other hand, the thermoelectric power Q of the UO_{2+x} cell was represented by the following equation [5]:

$$eQ = -d\gamma_h/dT = -e^{\times}\text{grad } V/\text{grad } T - \partial\mu_h/\partial T, \qquad (3\text{-}8)$$

where γ_h is the electrochemical potential of holes, grad V the potential gradient, μ_h the chemical potential of holes, and e and T have the usual meanings. In eq.(3-8) the term of $e^{\times}$grad V/grad T is assumed to be constant in this measurement. Then, the thermoelectric power depends on only the chemical potential of holes. It should be noticed that the large value of E in eqs.(3-6) and (3-7) corresponds to the state that the chemical potential of holes is low. Comparing eq.(3-6) with eq.(3-7) it is considered that the chemical potential of holes becomes low in accordance with the decomposition of the complexes. Consequently, from eq.(3-8) it is reasonably expected that the thermoelectric power decreases in the early stage of irradiation.

This concept that the oxygen interstitial-vacancy complexes are decomposed during irradiation qualitatively explains our results up to 1×10^{15} fissions/cm^3. Decomposition of the complexes into unassociated defects also supports the recovery of lattice strain at the beginning of irradiation, which has been already described in Chapt. 1. Of course, the trapping of holes with primary defects also contributes to the decrease of conductivity.

A thermoelectric power decrease was also found by Gevers et al.

up to about 1×10^{15} fissions/cm^3. These authors pointed out that the decrease of thermoelectric power was due to impurities changing the conduction mechanism to the n-type conduction, though the exact nature and origin of the impurities were not given.

At a certain dose, the steady state will be attained between the complexes in eq.(3-7) and the unassociated defects in eq.(3-6). Thus the thermoelectric power becomes almost constant in the dose range (1×10^{15} to 6×10^{17} fissions/cm^3), however, the electrical conductivity slightly increases. The behavior of thermoelectric power and electrical conductivity changes corresponds to the results of non-irradiated $UO_{2.003}$ in the temperature range from 700 to 1100 K by Wolfe [9]. The results of Wolfe was shown in fig.3-4. Possibly, the effect of irradiation was similar to that of temperature increase. If this is the case, it may be proposed that fission-induced vacancies and the incident heat produced by fission damage cause the lattice to relax, and as a result the energy lever of holes becomes shallow. Thus, this corresponds to the fact that holes become thermally activated.

The dose dependences of electrical conductivity and thermoelectric power at higher dose over 1×10^{18} fissions/cm^3 (i.e., the further increase of conductivity and decrease of thermoelectric power) also corresponded to the results reported by Wolfe [9], who observed a trend similar to our results for non-irradiated $UO_{2.003}$ in the intrinsic region above 1100 K. According to his

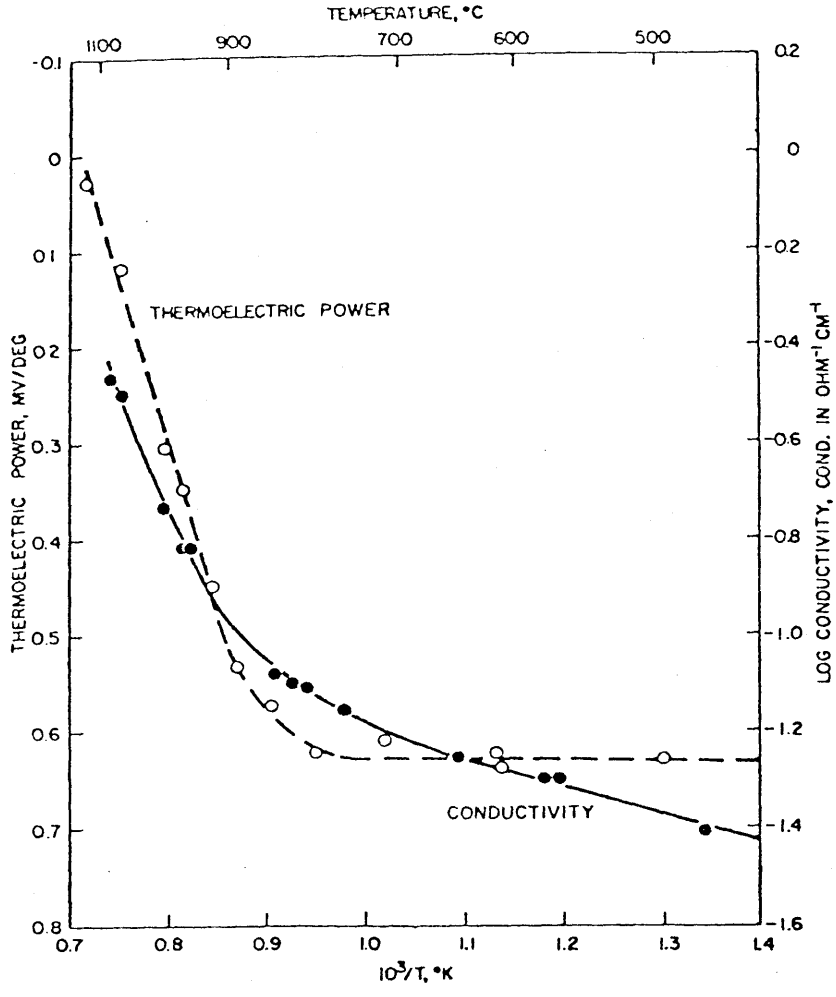

Fig.3-4. Temperature dependence of electrical conductivity and thermoelectric power in UO_2 by Wolfe [9].

report, at temperature above 1100 K (~800 °C) intrinsic conductivity with an energy gap of 1.9 eV was observed. Comparison of these results with the optical absorption data for UO_2 [16] showed a corresponding small absorption peak at 1.9 eV, indicating a narrow conduction band. The observation of the dose dependence of electrical properties at higher range, though only based on one data point, might indicate that at higher irradiation dose, the conductivity could change from extrinsic- to intrinsic-conductio due to the proposed mechanism above mentioned.

Roake [8] measured the electrical conductivity of UO_2 at higher doses, found an abrupt increase of conductivity (see fig.3-3) and concluded that this increase was due to a change from the p-type to the n-type. His speculation is in conflict with our result. However, it should be noted that the dose in his study was higher by an order of magnitude than in our investigation.

References

[1] W. Meyer, Z. Elektrochem. 50 (1944) 274.

[2] R. K. Willardson and J. W. Moody, in "Uranium Dioxide, Properties and Nuclear Applications", J. Belle ed. (1961).

[3] R. K. Wiilardson, J. W. Moody and H. L. Goering, J. Inorg. Nucl. Chem. 6 (1958) 19.

[4] R. R. Heikes and W. D. Johnston, J. Chem. Phys. 26 (1957) 582.

[5] S. Aronson, J. E. Rulli and B. E. Schaner, J. Chem. Phys. 35 (1961) 1382.

[6] H. M. Lee, J. Nucl. Mater. 50 (1974) 25.

[7] P. Nagels, W. Van Lierde, R. Penninckx, J. Devreese, M. Denayer, L. De Jonghe, R. De Coninck, R. De Batist, H. Blank, R. Gevers and S. Amelinckx, Geneva Conf., A / CONF. 28 / P / 444 (1964).

[8] W. E. Roake, "Radiation Damage in Reactor Materials, The Proceedings of The Symposium on Radiation Damage in Solids and Reactor Materials", p429 (1963) IAEA.

[9] R. A. Wolfe, WAPD-270 (1963).

[10] H. W. Russel, J. Amer. Ceramic Soc. 18 (1935) 1.

[11] P. Nagels, J. Derveese and M. Denayer, J. Appl. Phys. 35 (1963) 1175.

[12] S. Amerinckx (Supervisor), EUR 1414 e (1965).

[13] H. M. Lee, J. Nucl. Mater. 56 (1975) 81.

[14] B. T. M. Willis, Proc. Brit. Ceramic Soc. 1 (1964) 9.

[15] R. Gevers (Supervisor), EUR 3323 e (1967).

[16] D. M. Gruen, J. Amer. Chem. Soc. 76 (1954) 2117.

CHAPTER 4. IRRADIATION INDUCED LATTICE DEFECTS IN UO_2

4.1. Introduction

One of basic effects of irradiation in solids (pure metals, metal compounds and fissile materials) is displacement of atoms from their lattice sites, the resultant interstitials and vacancies being responsible for various radiation damage phenomena, including densification in UO_2. Kinchin-Pease [1] and Lindhard [2-5] models are available for the displacement of atoms. Using these models many investigators estimate the quantities of elementary lattice defects in metals irradiated by electron, fast neutron and heavy ions. But in the case of fissile materials the damage process is very complicated because it is the fission fragments damage. Consequently there is a few results concerning with the fission damage. Brinkmann [6] calculated the number of Frenkel pairs per fission in uranium metal. According to his calculation total of 5.8×10^5 Frenkel pairs are produced per fission event. Nelson [7] reported that the number of uranium atoms displaced per fission fragment in UO_2 is nearly one order of magnitude less than in pure uranium. Recently, MacEwen and Hastings [8] calculated the time-dependence of vacancy and interstitial concentrations for analyzing densification of UO_2 during irradiation using rate theory equations [9-12]. According to the rate theory equation the rate of defects concentration change is expressed as the difference between the production rate and the rates of annihilation and recombina-

tion.

In this paper concentrations of lattice defects such as interstitials and vacancies at various dose levels were estimated from changes of lattice parameter, density and porosity after irradiation mentioned in the previous chapters (Chapts. 1 and 2). An equation for dose dependence of the concentrations of lattice defects was also proposed. Moreover results obtained here, particularly to vacancy concentration, might be applied to diffusional properties such as diffusion, creep and densification. The application to irradiation-induced diffusion and creep is described in this chapter. Main purpose in this chapter is an estimation of the interstitial and vacancy concentrations from experimental data of lattice parameter, density and porosity on the basis of elastic continuum model in crystals.

4.2. Theoretical consideration

Concentrations of interstitials and vacancies are estimated from lattice parameter and bulk volume changes by following procedure: In a crystal of N_0 atoms, N_f displaced atoms are formed as Frenkel defects and end up in interstitial positions, while $(N_G + N_D + N_C + N_P)$ displaced atoms migrate to sinks during irradiation. N_G, N_D, N_C and N_P represent the numbers of atoms which go to grain boundaries, dislocations, clusters and pores, respectively, leaving a surplus of vacancies in the lattice. Since a Frenkel defect occupies the volume of a vacancy and an interstitial and a Schottky defect [a] that of a vacancy and a lattice atom, the overall bulk volume change due to these defects is

$$\Delta V_d = N_f(\Delta v_i + \Delta v_v) + N_G(\Delta v_v + \Omega) + N_D(\Delta v_v + \Delta v_D) + N_C(\Delta v_v + \Delta v_C) + N_P \Delta v_p, \quad (4\text{-}1)$$

where ΔV_d is bulk volume change after irradiation, Ω is the mean lattice atomic volume, Δv_v and Δv_i are decrease and increase of lattice atomic volume due to a vacancy and an interstitial, respectively, and Δv_D and Δv_C are volumes occupied by the displaced atoms which migrate to dislocations and clusters. ...

---

a) In this model, a Schottkt defect represents an isolated vacancy in one of the two sublattice with an adatom at a sink and/or at the surface.

Δv_p is volume change related to pore shrinkage. Though this cannot be exactly estimated, the probability of migration of displaced atoms to pores is expected to be very small in low dose range, that is,

$$N_P \Delta v_p \simeq 0.$$

In general, lattice atomic volume is defined as follows: unit cell volume is devided by total number of atoms which belong to the unit cell. For a compound such as UO_2, the values of Δv_v, Δv_i, Δv_D and Δv_C are also given as mean values. For simplicity of calculations the values of Δv_D and Δv_C are assumed to be Ω. Therefore, ΔV_d is rewritten in low dose range as follows,

$$\Delta V_d = N_f(\Delta v_v + \Delta v_i) + N_G(\Delta v_v + \Omega) + N_D(\Delta v_v + \Omega) + N_C(\Delta v_v + \Omega$$

$$= N_f \Delta v_i + (N_f + N_G + N_D + N_C)\Delta v_v + (N_G + N_D + N_C)\Omega.$$

When the sum of N_f, N_G, N_D and N_C is replaced by N,

$$\Delta V_d = N_f \Delta v_i + N \Delta v_v + (N - N_f)\Omega.$$

The original volume V is $N_0\Omega/(1 - P_0)$, hence,

$$\frac{\Delta V_d}{(1 - P_0)V} = \frac{N_f}{N_0}\frac{\Delta v_i}{\Omega} + \frac{N}{N_0}\frac{\Delta v_v}{\Omega} + \frac{N - N_f}{N_0}, \qquad (4\text{-}2)$$

where P_0 is a porosity for an original specimen.
N_f and N represent the numbers of interstitials and vacancies, respectively. The sum of N_G, N_D and N_C is equal to $(N - N_f)$ which corresponds to the number of excess vacancies (Schottky type defects). When the concentrations of interstitials, vacancies and excess vacancies (i.e., Schottky type defects) are represented by C_I, C_V and C_V', eq.(4-2) can be rewritten as

$$\frac{\Delta V_d}{(1 - P_0)V} = C_I(\Delta v_i/\Omega) + C_V(\Delta v_v/\Omega) + C_V' , \qquad (4\text{-}3)$$

where

$$C_V' = C_V - C_I. \qquad (4\text{-}4)$$

On the other hand, the volume change in the crystal lattice is given by

$$\Delta V' = N_f \Delta v_i + N \Delta v_v,$$

assuming that the defects which migrate outside the original lattice matrix do not contribute to the increase in volume of the crystal lattice. Since the number of lattice sites is N_0, the volume increase per lattice site (i.e., lattice volume) is given as follows

$$\Delta\Omega = \Delta V'/N_0 = (N_f/N_0)\,\Delta v_i + (N/N_0)\,\Delta v_v$$

$$= C_I \Delta v_i + C_V \Delta v_v. \qquad (4\text{-}5)$$

There is a simple relation between the lattice constant change, Δa, and the lattice volume change, $\Delta\Omega$:

$$\Delta\Omega/\Omega = 3(\Delta a/a). \qquad (4\text{-}6)$$

Inserting eq.(4-5) into the above relation gives

$$3(\Delta a/a) = C_I(\Delta v_i/\Omega) + C_V(\Delta v_v/\Omega). \qquad (4\text{-}7)$$

The values of $(\Delta v_i/\Omega)$ and $(\Delta v_v/\Omega)$ in eqs.(4-3) and (4-7) are estimated for UO_2 in Appendix 1. By inserting the estimated values of Δv_i (1.28Ω) and Δv_v (-0.27Ω) into eqs.(4-3) and (4-7), the following equations are obtained from the three equations, (4-3), (4-4) and (4-7) for the concentrations of interstitials (C_I), vacancies (C_V) and excess vacancies (C_V'):

$$C_I = 2.97(\Delta a/a) + 0.27\{(\Delta V_d/V)/(1 - P_0) - 3(\Delta a/a)\}, \qquad (4\text{-}8\text{-}1)$$

$$C_V = 2.97(\Delta a/a) + 1.27\{(\Delta V_d/V)/(1 - P_0) - 3(\Delta a/a)\}, \qquad (4\text{-}8\text{-}2)$$

and

$$C_V' = (\Delta V_d/V)/(1 - P_0) - 3(\Delta a/a). \qquad (4\text{-}8\text{-}3)$$

These equations (eqs.(4-8-1), (4-8-2) and (4-8-3)) are based on the assumption that both uranium and oxygen defects are produced in a certain proportion. Actually, oxygen defects are probably produced in much higher concentrations than uranium defects, and in this case the values of Δv_i and Δv_v are expected to be different from those mentioned above. As a result, the numerical coefficients of the first and second terms in eqs.(4-8-1) and (4-8-2) vary slightly, however, the values of C_I and C_V still remain with in the same order even if the Δv_i and Δv_v values vary within 10 %.

When pore shrinkage dominates in high dose range, the term of $N_P \Delta v_p$ in eq.(4-1) cannot be neglected. $N_P \Delta v_p$ and the bulk volume change in this case are described in detail in Appendix 2. According to Appendix 2, eq.(4-3) can be rewritten by

$$\frac{(1 - P)\Delta V_d}{(1 - P_0)V} - \frac{P - P_0}{1 - P_0} = C_I(\Delta v_i/\Omega) + C_V(\Delta v_v/\Omega) + C_V', \quad (4\text{-}9)$$

where P is a post-irradiation porosity.
In order to estimate C_I and C_V in this case, the left-hand side of eq.(4-9) should be inserted in eqs.(4-8-1) and (4-8-2) instead of $\Delta V_d/V(1 - P_0)$. Then, the following two equations are given for C_I and C_V in this case:

$$C_I = 2.97(\Delta a/a) + 0.27\left\{\frac{(1 - P)\,\Delta V_d}{(1 - P_0)V} - \frac{P - P_0}{1 - P_0} - 3(\Delta a/a)\right\},$$

(4-10-1)

and

$$C_V = 2.97(\Delta a/a) + 1.27\left\{\frac{(1 - P)\,\Delta V_d}{(1 - P_0)V} - \frac{P - P_0}{1 - P_0} - 3(\Delta a/a)\right\}.$$

(4-10-2)

4.3. Results

The concentrations of interstitials and vacancies are obtained using eqs.(4-8-1), (4-8-2), (4-10-1) and (4-10-2) as shown in fig.4-1 for the dose range up to 2×10^{18} fissions/cm^3. The concentrations of these defects at higher dose range (over 5.6×10^{16} fissions/cm^3) which are calculated using eqs.(4-10-1) and (4-10-2) are less reliable than those at lower dose range because there are less data points in the pore analysis.

The interstitial concentration increases with fission dose and is saturated at about 1×10^{16} fissions/cm^3. After this dose, it increases again and is saturated at about 3×10^{17} fissions/cm^3 and about 1×10^{17} fissions/cm^3 for the specimens of 5 and 2.5 μm grain sizes, respectively. At higher dose range over about 3×10^{17} fissions/cm^3 the interstitial concentration abruptly decreases. The interstitial concentration in the specimen with smaller grain size is saturated earlier with lower values than that with larger grain size. These trends are similar to those of lattice parameter. On the other hand, the vacancy concentration gradually increases with dose to 5×10^{15} fissions/cm^3. In the dose range where the saturation of both interstitial concentration and lattice parameter continues in the first stage, the vacancy concentration continues to increase and is saturated. After saturation the vacancy concentration seems to decrease gradually, and the behavior of the decrease is different between two kinds

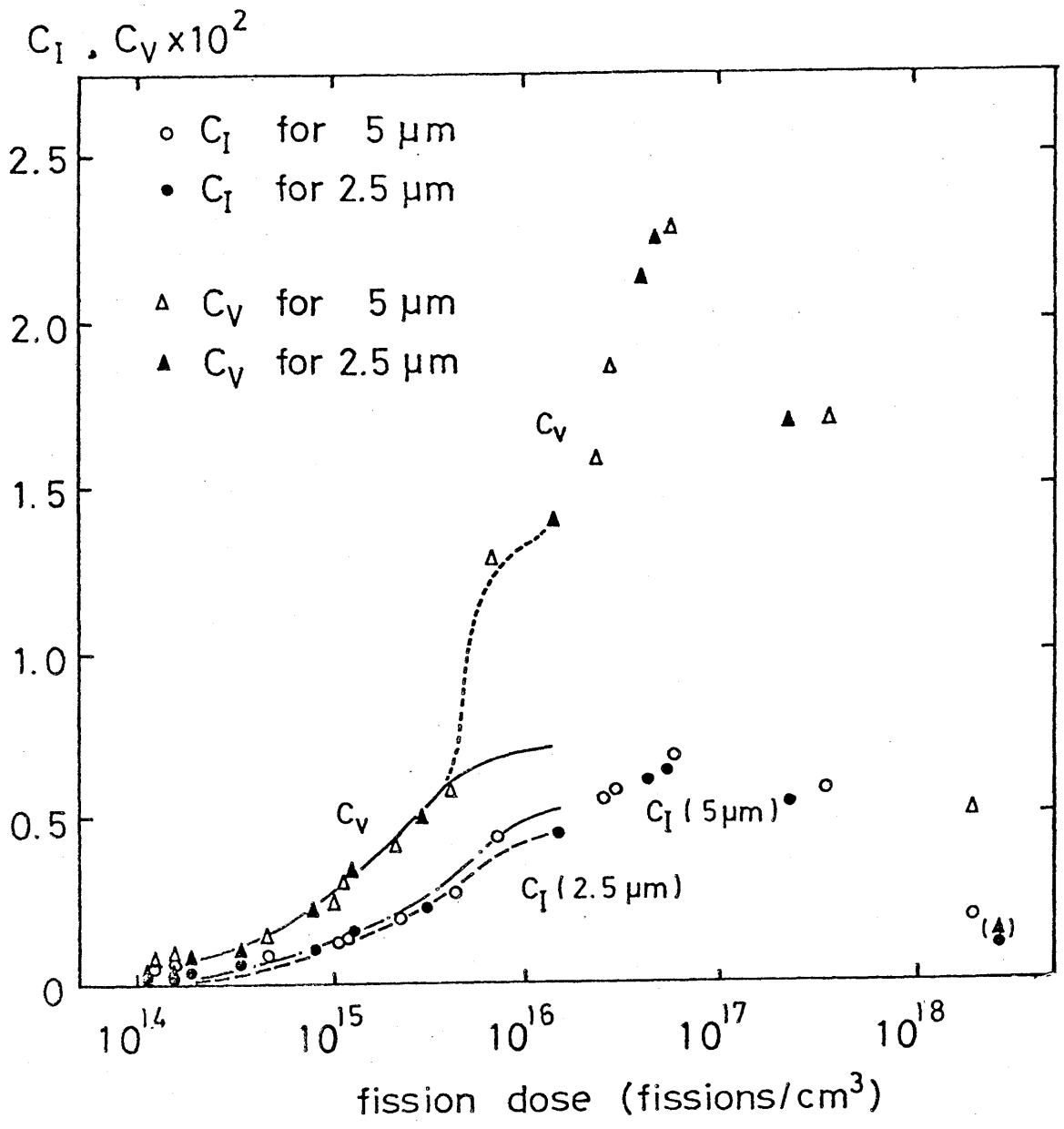

Fig.4-1. Variation of the concentrations of vacancies and interstitials versus fission dose. Solid curves representing the vacancy concentration for both specimens of 2.5 and 5 μm grain sizes were calculated by means of eq.(4-14). The dot-dash curve represents the concentration of interstitials for specimen of 5 μm grain size, and the broken curve that for specimen of 2.5 μm. These curves for C_I were calculated by means of eq.(4-12).

of specimens of 2.5 and 5 μm grain sizes.

The dose dependence of the concentrations of interstitials and vacancies is predicted in the low dose range using the first order kinetic equation as follows:
For the interstitial concentration (C_I),

$$dC_I/dt = V_I \Sigma_f \phi_{th}(1 - C_I), \qquad (4\text{-}11)$$

where V_I is an effective volume for producing interstitials per fission event, and Σ_f, ϕ_{th} and t have the usual meanings. By integrating eq.(4-11) with the boundary condition, $C_I = 0$ at $t = 0$, the following equation is obtained,

$$C_I = C_I^s \left\{1 - \exp(-V_I \Sigma_f \phi_{th} t)\right\} , \qquad (4\text{-}12)$$

where C_I^s is the concentration of interstitials at saturation. Values of C_I^s and V_I were calculated by applying a least square method to the eq.(4-12). Estimated values of C_I^s and V_I up to 1×10^{16} fissions/cm^3 are indicated in table 4-1.
For the vacancy concentration (C_V),

$$dC_V/dt = V_V \Sigma_f \phi_{th}(1 - C_V), \qquad (4\text{-}13)$$

where V_V is a constant similar to V_I. By integrating eq.(4-13) with the boundary condition, $C_V = 0$ at $t = 0$,

le 4-1 Saturation values of C_I and C_V and effective volumes for producing interstitials and vacancies based on a first order kinetic reaction per fission event for both specimens of 2.5 and 5 μm grain sizes.

	C_I^s	C_V^s	$V_I(cm^3)$	$V_V(cm^3)$
μm	4.5×10^{-3}	0.75×10^{-2}	3.22×10^{-16}	4.15×10^{-16}
ιm	5.5×10^{-3}	0.75×10^{-2}	2.97×10^{-16}	4.15×10^{-16}

$$C_V = C_V^S \left\{1 - \exp(-V_V \Sigma_f \phi_{th} t)\right\} , \qquad (4\text{-}14)$$

where C_V^S is the vacancy concentration at saturation. Values of C_V^S and V_V are obtained by the procedure similar to that for C_I^S and V_I, and these values are also shown in table 4-1. The fitting curves obtained by use of eqs.(4-12) and (4-14) are illustrated in fig.4-1. The prediction of the dose dependence of the concentrations in high dose range cannot be done for lack of data points.

4.4. Discussion

Both the concentrations of interstitials and vacancies increased with fission dose up to about 1×10^{17} fissions/cm^3. In this dose range, the vacancy concentration increased faster than that of interstitials, probably because some of interstitials migrated to sinks such as grain boundaries and dislocations. The rapid increase of vacancy concentration was observed in the dose range between 4×10^{15} and 1×10^{16} fissions/cm^3 as illustrated with dotted line in fig.4-1. Since the first saturation of interstitials occurs in this range and continues to the dose where the secondary interstitials begin to be produced, author suggests that in this stage almost all interstitials migrate to sinks, especially to clusters. Interstitial clusters had been observed by Whapham and Sheldon [13] with electron microscope in this dose range. Furthermore, considering no lattice parameter change, the vacancies also must form clusters. However, vacancy clusters have not been observed in this dose range by electron microscope [13,14]. Therefore, two cases are suggested. (1). The size of the vacancy clusters is too small to distinguish the nature. (2). The vacancy clusters might be absorb interstitials from the beginning of their origin and form interstitial clusters. Author supposes the second case might be probable. Anyhow, C_V calculated by eq.(4-8-2) above this stage is an apparent concentration as that of isolated vacancies. Possibly, the concentration of isolated vacancies should be smaller than the calcu-

lated concentration.

The decrease of the interstitial concentration in higher dose was due to the annihilation with vacancies mentioned in Chapt. 1. The same trend of vacancies in high dose seemed to contradict to the model for the third stage of lattice parameter change in Chapt. 1. In that model the vacancy concentration increased to saturation. This contradiction may be explained as follows: The vacancy concentration calculated by eq.(4-10-2) in higher dose was also an apparent concentration as that of isolated vacancies as mentioned above. Probably the calculated vacancy concentration involves both concentrations of vacancies which exist in the lattice matrix and outside of the lattice. The former type of vacancies almost correspond to interstitials, and, therefore, it is supposed that the number of the former type of vacancies is much less than that of the latter type. The apparent decrease of the vacancy concentration is possibly related to the bulk volume decrease which is due to annihilation of interstitial clusters. Consequently the effect of the annihilation of interstitial clusters in higher dose, the concentration of vacancies which exist outside of the lattice might decrease. Considering the observation of vacancy clusters by Whapham and Sheldon [13] and Golyanov and Pravdyuk [14] in electron microscope, these vacancies tend to be clustering. As a result, the apparent concentration of vacancies decreases. On the other hand, the former type of vacancies (i.e., isolated vacancies existing in

the lattice matrix) is expected to increase to the saturation.

In order to estimate irradiation-induced diffusion and creep, the uranium vacancy concentration must be calculated. Vacancy concentration in thermal equilibrium is generally given as

$$C_V^e = \exp(\Delta s/k)\exp(-E_f/kT), \qquad (4\text{-}15)$$

where the first exponential term is the entropy factor and E_f is the formation energy of a vacancy. In calculating the vacancy concentration in UO_2, the value of 10 was taken for the entropy factor of both uranium and oxygen vacancies, and 2.1 eV [15,16] and 1.3 eV [15,17] were used for the formation energies of uranium and oxygen vacancies, respectively. Both energies for hyper-stoichiometric UO_2 were estimated by use of the following relation:

$$E_f = Q - E_m,$$

where E_f, E_m and Q are the activation energies of vacancy formation, migration and diffusion, respectively. E_m for uranium and oxygen in UO_2 has been determined experimentally by other workers [12] as 2.4 eV and 1.3 eV, respectively, and Q was chosen in the aboundant thermal diffusion data in UO_2 [16-25] as 4.5 eV and 2.6 eV for uranium and oxygen, respectively.

If the irradiation-produced vacancy concentration (C_V^{irr}) would be correspond to that in thermal equilibrium, the following relation

is held:

$$10\exp(-2.1/kT) + 10\exp(-1.3/kT) = C_V^{irr}, \qquad (4\text{-}16)$$

where the first and second terms correspond to the concentrations of uranium and oxygen vacancies, respectively, and C_V^{irr} is calculated by eqs.(4-8-2) and (4-10-2). By solving eq.(4-16), the temperature calculated at various doses. The temperature calculated above will be called the "corresponding temperature". Putting the "corresponding temperature" into the first term of eq.(4-16), the concentration of uranium vacancies is obtained. The concentration and the "corresponding temperature" were plotted as a function of dose in fig.4-2.

MacEwen and Hastings [87] had calculated the concentrations of interstitials and vacancies of uranium in irradiated UO_2 at 900 K. Their calculations showed that in very short irradiation time the concentrations of interstitials and vacancies increased at the same rate. Then, the interstitial decreased rapidly while the vacancy increased slowly to a steady state value. However, their calculations may be misleading because they used a too small migration energy (0.3 eV) for uranium interstitials.

The irradiation-induced diffusion coefficient was estimated as follows: It was assumed that the migration of uranium vacancies was enhanced by the irradiation, and the irradiation-

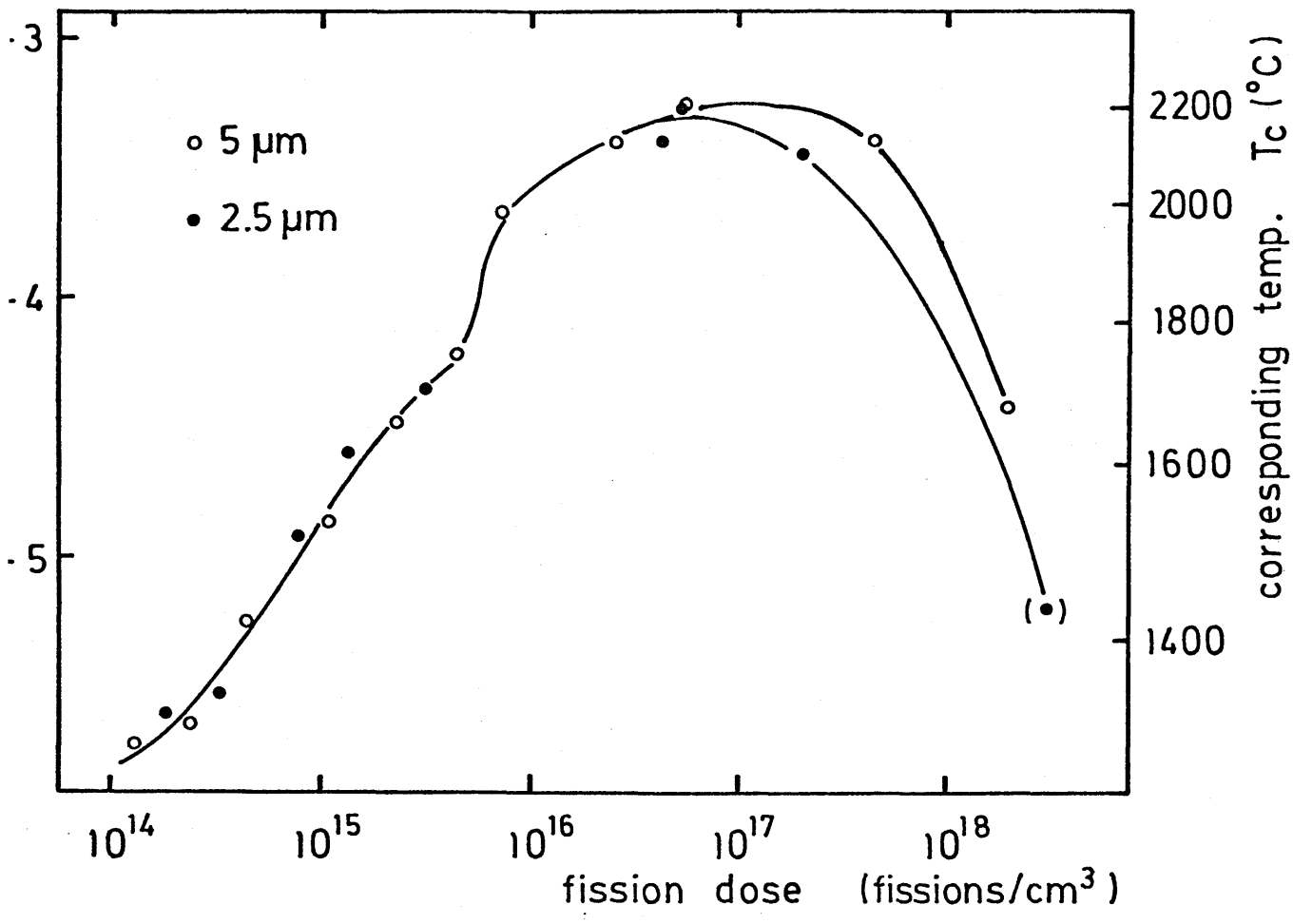

Fig.4-2. Variation of uranium vacancy concentration versus fission dose. These are calculated by using eq.(4-16).

induced diffusion coefficient might be obtained by putting the "corresponding temperature" into the usual diffusion equation; the procedure is based on the assumption that lattice atoms are relaxed by irradiation. This assumption will be supported by the measurement of Debey Temperature decrease in irradiated UC [26]. Therefore, the irradiation-induced diffusion coefficient of uranium is obtained as

$$D_U^{th} = \nu\, C_{VU}^{th} \exp(-E_m/kT), \tag{4-17}$$

$$D_U^{irr} = \nu\, C_{VU}^{irr} \exp(-E_m^{irr}/kT), \tag{4-18}$$

$$= \nu\, C_{VU}^{irr} \exp(-E_m/kT_c), \tag{4-19}$$

where D_U^{th} and D_U^{irr} are the thermal and irradiation-induced diffusion coefficients of uranium, ν is jumping frequency, C_{VU}^{th}, C_{VU}^{irr} are the thermal and irradiation-produced vacancy concentration of uranium, and E_m^{irr} is the migration energy under irradiation. The dose dependence of the irradiation-induced diffusion coefficient are shown in fig.4-3. The comparison of it with the data of other workers [27-30] are indicated in fig.4-4. Many workers considered that the irradiation-induced diffusion depended on mainly fission rate, while the present study showed that it depended on total fission dose (i.e., the vacancy concentration). They considered that the irradiation-induced diffusion was caused by the atom diffusion along fission spike (i.e., short circuit

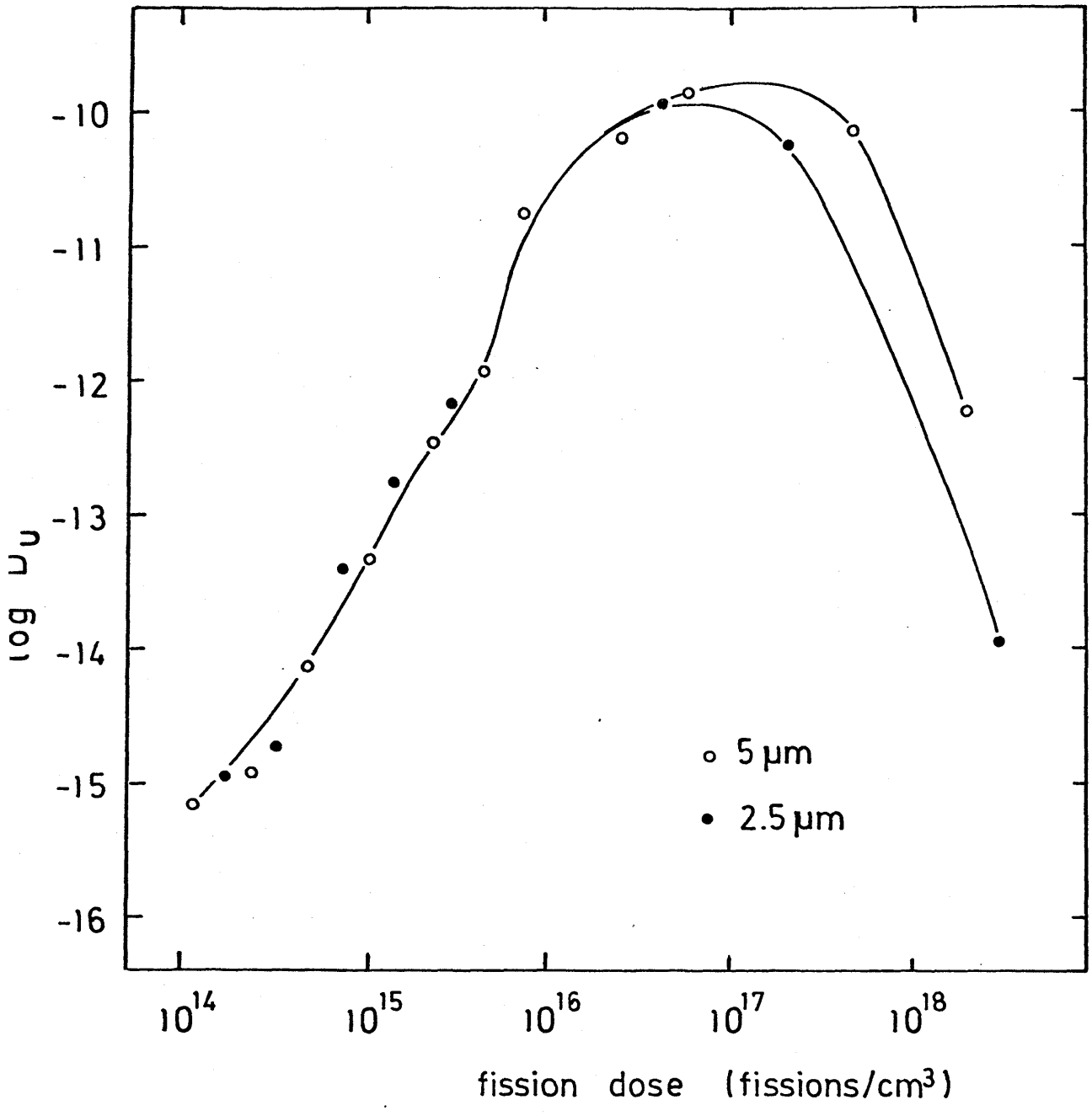

Fig.4-3. Irradiation-induced diffusion coefficient of uranium at various fission dose. These are calculated by using eq.(4-19).

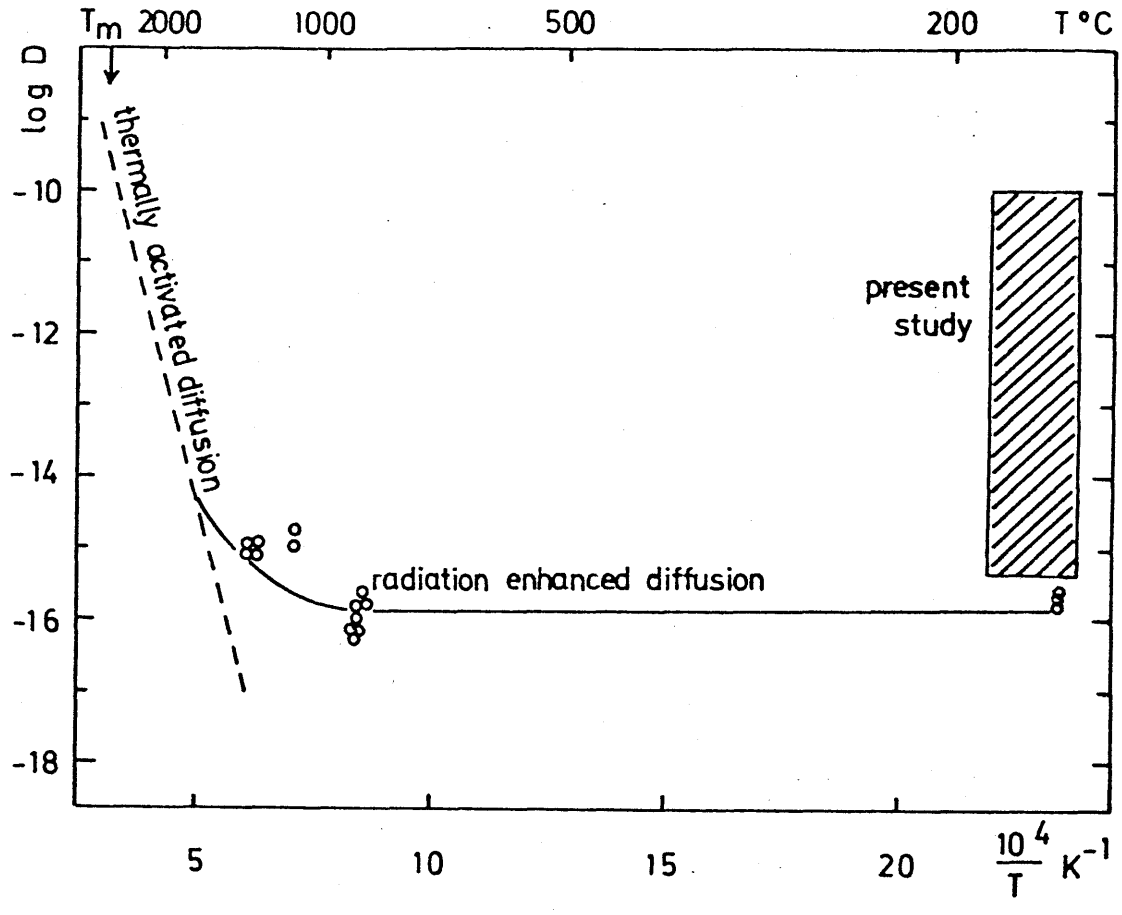

Fig.4-4. The comparison of the irradiation-induced diffusion coefficient of uranium in UO_2 with the data of other worker [30].

diffusion). On the contrary, it is considered in this paper that the irradiation-induced diffusion occurs due to high concentration of vacancies.

The irradiation-induced diffusion coefficient estimated above was applied to the irradiation-induced creep behavior. The irradiation-induced creep rate is represented as follows using Herring-Nabbaro formula [31],

$$\dot{\varepsilon}_{irr} = 20\sigma b^3 D_U^{irr}/L^2 kT, \qquad (4\text{-}20)$$

where $\dot{\varepsilon}_{irr}$ is the irradiation-induced creep rate, σ an applied stress, b a distance between atoms, D_U^{irr} the irradiation-induced diffusion coefficient of uranium estimated above, L the grain size, and k and T have the usual meanings. The irradiation-induced creep rate can be calculated by use of values of σ, b, L, T (which are shown in table 4-2) and D_U^{irr}. The calculated creep rates by eq.(4-20) were plotted in fig.4-5 together with the experimental data of Clough [32]. This figure showed that the creep rate decreased with increasing dose in high dose range, and it depended remarkably on grain size. In addition, since the trend of the estimated creep rate corresponds to that of the experimental results of creep rate, the estimation of irradiation-induced diffusion coefficients, D_U^{irr}, in this paper might be reasonable.

Table 4-2 Parameters, σ , b, L and T which are used in calculating creep rate.

σ	20 MN/m^2
b	0.7×10^{-10} m
L	5 μm
T	150 ^{o}C

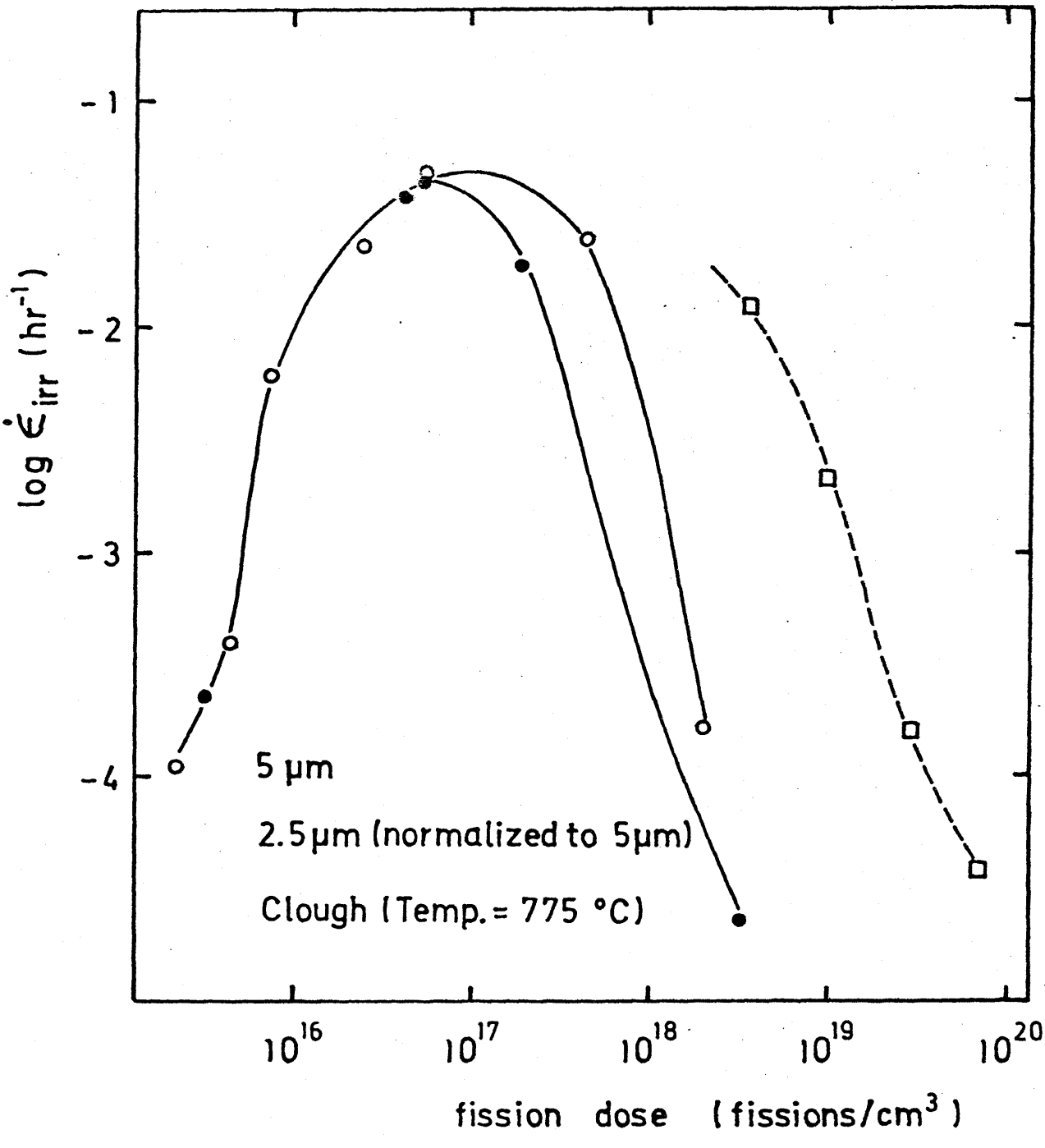

Fig.4-5. The calculated creep rate by means of eq.(4-20) together with the experimental data of Clough [32].

References

[1] G. H. Kinchin and R. S. Pease, Rep. Prog. Phys. 18 (1955) 1.

[2] J. Lindhard and M. Scharff, Phys. Rev. 124 (1961) 128.

[3] J. Lindhard and P. V. Thomsen, in "Radiation Damage in Solids, vol.1", Proc. Symp. IAEA (1962) p65.

[4] J. Lindhard, V. Nielsen, M. Scharff and P. V. Thomsen, Kgl. Danske Vidensk. Selsk. Mat.-Fys. Medd. 33 (1963) No.14.

[5] J. Lindhard, M. Scharff and H. E. Schiøtt, ibid. 33 (1963) No.10.

[6] J. A. Brinkmann, in D. S. Billington (ed.), "Radiation Damage in Solids", Proc. Int. School of Phys. ENRICO FERMI, Academic Press, New York and London, (1962) p830.

[7] R. S. Nelson, J. Nucl. Mater. 25 (1968) 227.

[8] S. R. MacEwen and I. J. Hastings, Phil. Mag. 31 (1975) 135.

[9] S. D. Harkness and C. Li, Metall. Trans. 2 (1971) 1457.

[10] H. Wiedersich, Radiat. Effects, 12 (1972) 111.

[11] A. D. Brailsford and R. Bullough, J. Nucl. Mater. 44 (1972) 121.

[12] R. Bullough, B. L. Eyre and R. C. Perrin, Nucl. Appl. Tech. 9 (1970) 346.

[13] A. D. Whapham and B. E. Sheldon, Phil. Mag. 11 (1965) 1179.

[14] V. M. Golyanov and N. F. Pravdyuk, 3rd UN Conference, Geneva 1964, paper A / Conference 28 / P / 338 (1965).

[15] Hj. Matzke, AECL-2585 (1966).

[16] R. Lindner and F. Schmitz, Z. Naturf. 169 (1961) 1373.

[17] J. F. Marin and P. Contamin, J. Nucl. Mater. 30 (1969) 16.

[18] A. B. Auskern and J. Belle, ibid. 3 (1961) 267.

[19] W. Dornelas and P. Lacombe, ibid. 21 (1967) 100.

[20] P. Contamin and R. Stefani, CEA-R-3179 (1967).

[21] R. J. Hawkins and C. B. Alcock, J. Nucl. Mater. 26 (1968) 112.

[22] S. Yajima, H. Furuya and T. Hiroi, ibid. 20 (1966) 162.

[23] J. Belle, ibid. 30 (1969) 3.

[24] Hj. Matzke, ibid. 30 (1969) 26.

[25] D. K. Reimann and T. S. Lundy, Amer. Ceram. Soc. 52 (1969) 511.

[26] M. Mori, private communication.

[27] M. L. Bleiberg, J. Nucl. Mater. 1 (1959) 182.

[28] Hj. Matzke, Topical Meeting Proc., Advanced LMFBR Fuels, ERDA 4455 (1977) p218.

[29] W. Dienst, KFK-1215 and AECL-4375 (1970).

[30] Hj. Matzke, private communication.

[31] F. R. N. Nabarro, Report Conf. Strength of Solids (London, The Physical Society, 1948) 75.

[32] D. J. Clough, J. Nucl. Mater. 56 (1975) 279.

[33] J. D. Eshelby, J. Appl. Phys. 25 (1954) 255.

[34] I. J. Fritz, J. Appl. Phys. 47 (1976) 4353.

[35] L. Tewordt, Phys. Rev. 109 (1958) 61.

[36] R. A. Johnson and E. Brown, Phys. Rev. 127 (1962) 446.

Appendix 4.1. Estimation of the values of Δv_i and Δv_v

In view of the elastic continuum model, Eshelby [33] deduced the following relations for Δv_i and Δv_v:

$$\Delta v_i = 4\pi r_0^2 \delta_{0i} \frac{3(1 - \sigma)}{1 + \sigma} ,$$

and

$$\Delta v_v = 4\pi r_0^2 \delta_{0v} \frac{3(1 - \sigma)}{1 + \sigma} ,$$

where r_0 is the nearest-neighbor separation distance in the perfect lattice, σ Poisson's ratio and δ_{0i} and δ_{0v} are the displacements at a center of dilatation and contraction, respectively. It is assumed that both U and O defects in UO_2 are produced in a certain proportion of the components. The values of r_0 is $(\sqrt{3}/4)a$ as shown in table A.4-1 and corresponds to the separation distance between uranium and oxygen atoms.
The values of δ_{0i} and δ_{0v} for UO_2 could not be found in the literature and were, therefore, estimated by comparison of the bulk modulus of UO_2 [34] with that of copper. The values of δ_{0i} and δ_{0v} for copper were theoretically calculated by Tewordt [35] and Johnson and Brown [36]. The values of σ, δ_{0i}, δ_{0v}, Δv_i and Δv_v for uranium dioxide are summarized in table A.4-1.

Table A.4-1 Parameters σ, r_0, δ_{0i}, δ_{0v}, Δv_i and Δv_v in UO_2. The values of δ_{0i} and δ_{0v} were estimated from the bulk modulus of UO_2 (2.10×10^{11} N/m^2) [34] compared with that of Cu (1.35×10^{11} N/m^2). The relation $\Omega = a^3/12$ has been found to hold in UO_2 where a is the lattice parameter and Ω is the lattice atomic volume.

σ	r_0(Å)	δ_{0i}(Å)	δ_{0v}(Å)	Δv_i(Å^3)	Δv_v(Å^3)
0.3	$(\sqrt{3}/4)a$	0.028a	-0.006a	1.28Ω	-0.27Ω

Appendix 4.2. Bulk and pore volume changes due to pore shrinkage in a high dose range

In this paper, it is assumed that pore shrinkage resulting densification in high dose range is due to irradiation-induced diffusion of lattice atoms to pores. In this case, N_P in eq.(4-1) contains both displaced atoms and lattice atoms which migrate to pores during irradiation. When N_P atoms migrate to pores, the corresponding vacancies are left at the surface and/or in the lattice matrix. The numbers of vacancies at each site are represented by N_{P1} and N_{P2}, respectively, where

$$N_P = N_{P1} + N_{P2}.$$

It is assumed that the former type of vacancies decreases the bulk volume by $(-\Omega)$, and the latter by Δv_v. Then, $N_P \Delta v_P$ in eq.(4-1) can be expressed by

$$N_P \Delta v_P = N_{P1}(-\Omega) + N_{P2} \Delta v_v.$$

Therefore, the bulk volume change (ΔV_d) is given by

$$\Delta V_d = N_f \Delta v_i + (N_f + N_G + N_D + N_C + N_{P2}) \Delta v_v$$

$$+ (N_G + N_D + N_C)\Omega + N_{P1}(-\Omega)$$

$$= N_f \Delta v_i + N \Delta v_v + (N - N_f - N_{P2})\Omega + N_{P1}(-\Omega)$$

$$= N_f \Delta v_i + N \Delta v_v + (N - N_f)\Omega - N_P\Omega, \qquad \text{(A.4-1)}$$

where

$$N = N_f + N_G + N_D + N_C + N_{P2}.$$

N corresponds to the number of vacancies in the lattice.

On the other hand, the pore volume change (ΔV_p) is given by

$$\Delta V_p = N_P(-\Omega). \qquad \text{(A.4-2)}$$

From eqs.(A.4-1) and (A.4-2), we obtain the following equation:

$$\Delta V_d = N_f \Delta v_i + N \Delta v_v + (N - N_f)\Omega + \Delta V_p$$

i.e.,

$$\Delta V_d - \Delta V_p = N_f \Delta v_i + N \Delta v_v + (N - N_f)\Omega. \qquad \text{(A.4-3)}$$

The original bulk volume V is $N_0\Omega/(1 - P_0)$, hence, eq.(A.4-3) is rewritten by

$$\Delta V_d/(1 - P_0)V - \Delta V_p/(1 - P_0)V = C_I(\Delta v_i/\Omega) + C_V(\Delta v_v/\Omega) + C_V', \qquad \text{(A.4-4)}$$

where

$$C_V' = C_V - C_I.$$

Eq.(A.4-4) indicates that the difference between the fractional bulk volume change ($\Delta V_d/V$) and the fractional pore volume change ($\Delta V_p/V$) is due to defects and defect clusters.

While, the pore volume change can be expressed using a porosity obtained by pore analysis as follows:

$$\Delta V_p = P(V + \Delta V_d) - P_0 V,$$

i.e.,

$$\Delta V_p/V = (P - P_0) + P(\Delta V_d/V). \qquad (A.4\text{-}5)$$

By inserting eq.(A.4-5) into eq.(A.4-4) we obtained the following relation:

$$\frac{1 - P}{1 - P_0}\frac{\Delta V_d}{V} - \frac{P - P_0}{1 - P_0} = C_I(\Delta v_i/\Omega) + C_V(\Delta v_v/\Omega) + C_V', \qquad (A.4\text{-}6)$$

which is equation (4-9).

Nomenclatures

N_0 : the number of atoms in the original crystal

N_f : the number of atoms which form a Frenkel defect

N_G : the number of atoms which migrate to grain boundaries

N_D : the number of atoms which migrate to dislocations

N_C : the number of atoms which migrate to clusters

N_P : the number of atoms which migrate to pores

N_{P1} : the number of atoms which migrate to pores leaving a surplus vacancy at the surface

N_{P2} : the number of atoms which migrate to pores leaving a surplus vacancy in the lattice matrix

N : the sum of N_f, N_G, N_D and N_C in the low dose range

N : the sum of N_f, N_G, N_D, N_C and N_{P2} in the high dose range

: a mean lattice atomic volume

Δv_i : the increase of lattice atomic volume due to an interstitial

Δv_v : the decrease of lattice atomic volume due to a vacancy

Δv_P : the volume change due to pore shrinkage

ΔV_d : bulk volume change due to defects and defect clusters

ΔV_p : pore volume change due to pore shrinkage

P_0 : pre-irradiation porosity

P : post-irradiation porosity

C_I : interstitial concentration

C_V : vacancy concentration

C_V' : excess vacancy concentration (Schottky type defect concentratic

CHAPTER 5. IRRADIATION INDUCED DENSIFICATION IN UO_2

5.1. Introduction

In 1972 densification, which means that UO_2 fuel pellets densify during irradiation, was observed in Presurized Water Reactors (PWRs) (Ginna, Beznau, Point Beach and Robinson reactors) [1-4]. The densification makes the increase of pellet temperatures caused by radial shrinkage and flux peaking due to axial gaps in the fuel column.

The fuel densification depends on its microstructure, total fission dose and temperature during irradiation. Parametric surveies of these dependences have been carried out by a vast investigators [5-20]. For example, Chubb et al. [5] reported that in-pile densification could be controlled by the microstructure of the fuel, particularly its pore size distribution and porosity. Ferrari et al. [16] showed that the fuel densification occurred quite rapidly at the initial stage of irradiation and was saturated at approximately 6000 MWD/TU. According to ref.[19], sintering porosity was removed with densification in pile at lower temperatures than those for out of pile thermal sintering. Hastings [20] pointed out that densification occurred in the two temperature regions except the midle of the three (i.e., (1) at $\lesssim$1300 K, where densification occurred, (2) from 1300 to 1900 K, where swelling predominated and (3) at $\gtrsim$ 1900 K, where swelling

and densification were observed) in irradiated UO_2 pellets.

Many theories have been proposed [8,21-25] to explain the in-pile densification. It is reasonably considered that the densification depends on irradiation-enhanced diffusion [21]. However, other concepts are proposed for the densification by Carlson [22], Stehle and Assmann [23,24] and MacEwen and Hastings [25]. The models of these authors will be described in the section 5.3.2.. Though many models are probable, an available explanation to the in-pile densification has not been made at present. In addition, reasonable explanation of dose dependence of densification is scarce.

In this chapter, a model for densification is proposed, and we try to make a prediction of the dose dependence of densification. To such purpose two sets of UO_2 specimens with different microstructures are irradiated up to a dose about 2×10^{19} fissions/cm^3 (corresponding to about 1000 MWD/ton UO_2) and the changes of bulk density, porosity and pore size distribution are investigated.

5.2. Experimental

Specimens used in this study are the same as those for lattice parameter, density and electrical properties measurements. The microstructures of the specimens are shown in photo 5-1. As shown in these photographs, specimen with the grain size of 2.5 μm has many small pores less than 1 μm, while specimen with 5 μm grain size has less.

The irradiation procedure up to 3×10^{18} fissions/cm^3 has been already described in detail in Chapt. 1 (section 1.2.2). The highest irradiations (about 2×10^{19} fissions/cm^3) were performed to specimens, which have 10 mm diameter and 2 mm of thickness, by using JMTR (Japan Material Testing Reactor) with a thermal neutron flux of about 1.5×10^{14} cm^{2}sec^{-1}. The irradiation temperature in JMTR was estimated to be at most 300 °C, because surface temperature of the cludding was measured to be about 70 °C and the UO_2 disks were sandwiched with stainless steel and in this case heat release from the UO_2 pellets would be expected to be large.

Porosity measurements have been already described in Chapt. 2 (section 2.2.2).

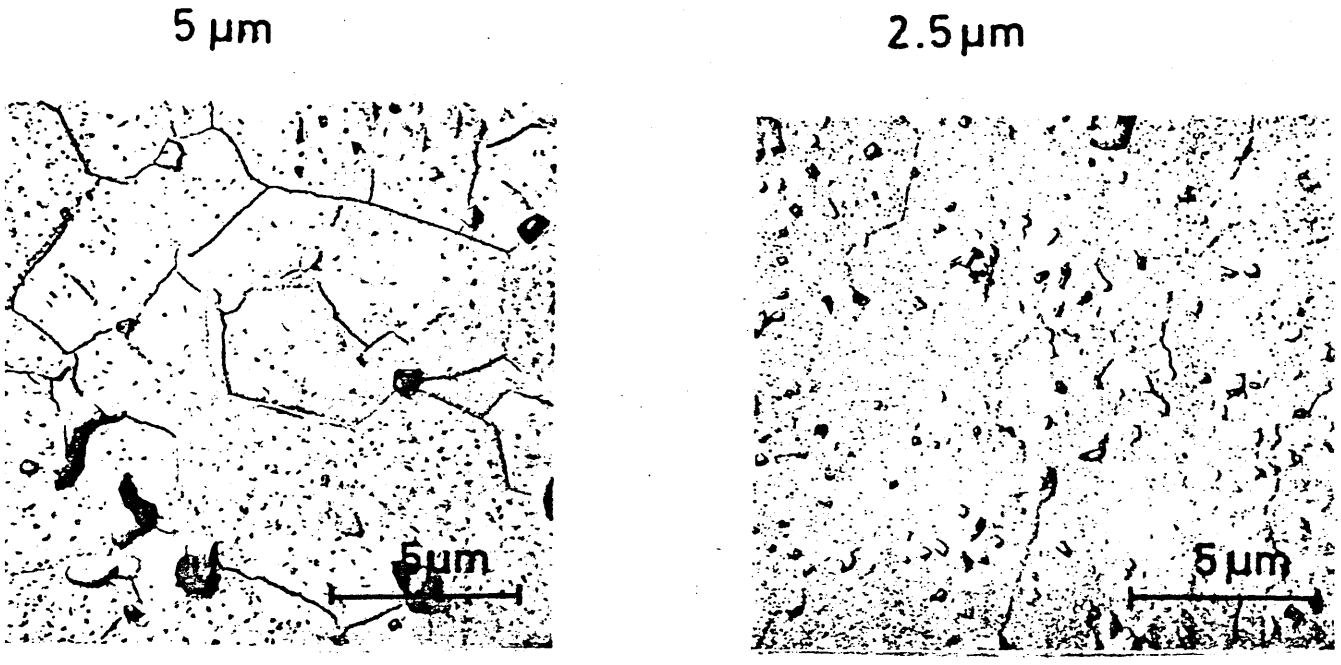

Photo 5-1. Microstructure of both specimens of 5 and 2.5 μm grain sizes, respectively, before irradiation.

5.3. Results and discussion

5.3.1. Porosity change after irradiation

Figs.5-1 and 5-2 show pore size distribution of pre- and post-irradiated samples of 2.5 and 5 μm grain sizes, respectively. Removal of pores of less than 10 μm in diameter is clearly observed. This result is good agreement with those reported by other workers [5,16]. Our analysis, however, showed that pores having more than 10 μm in diameter tended to shrink.

Porosity changes after irradiation are summarized in table 2-2. The pore volume change has been already described in the chapter 2 in connection with the bulk volume changes.

Though the exact mechanism for pore annihilation is still unknown, the kinetics of pore annihilation are proposed on the basis of irradiation enhanced diffusion process [26-30]. Our proposal on pore annihilation is that lattice atoms and displaced atoms easily migrate to pores due to irradiation-induced diffusion. This might be supported by the fact that removal of pore starts apparently at a dose where vacancy concentration is enough high to enhance the diffusion during irradiation. The irradiation-induced diffusion has been mentioned in the preceding chapter (Chapt. 4).

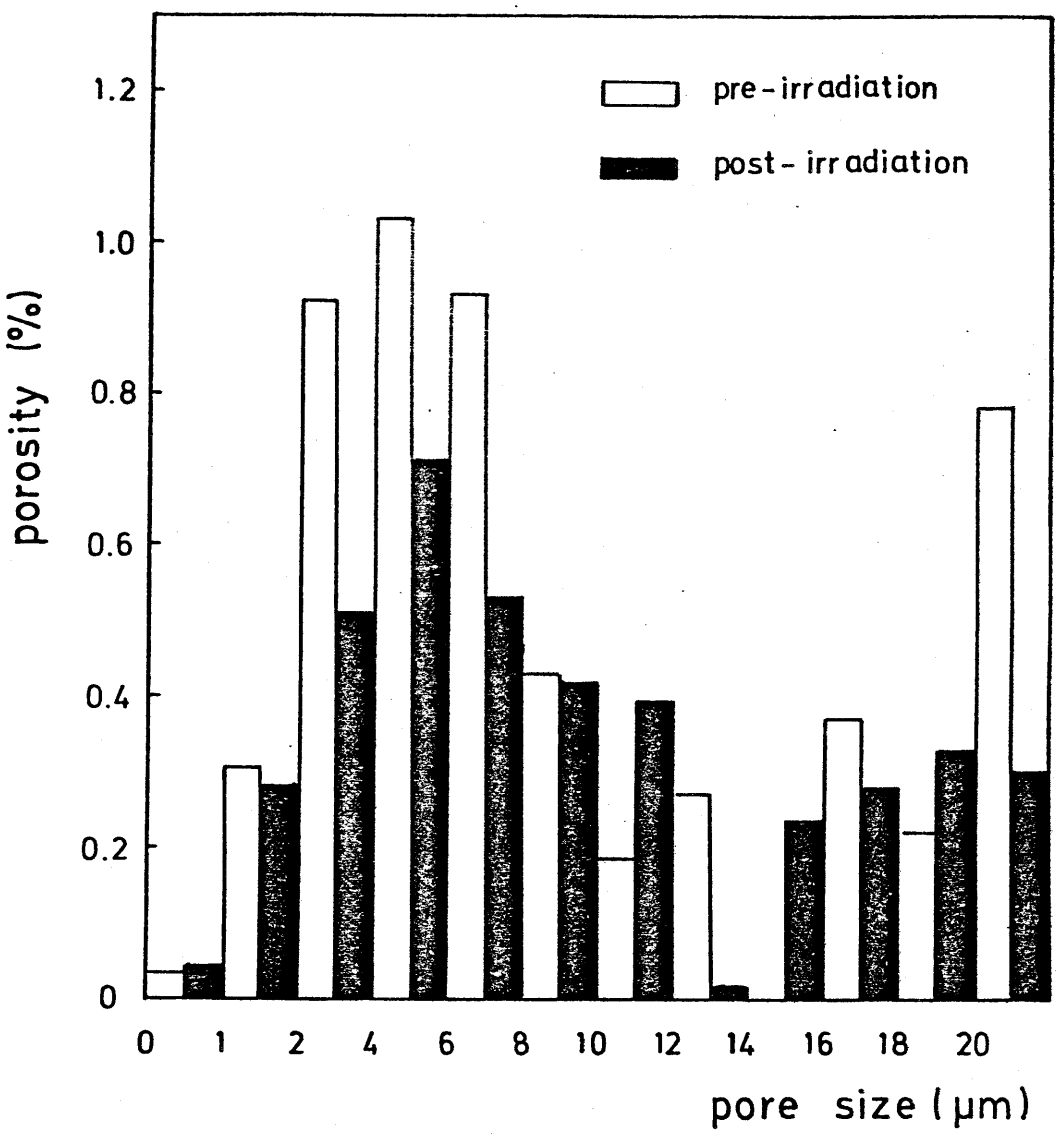

Fig.5-1. Pore size distribution of pre- and post-irradiation sample of 5 μm grain size.

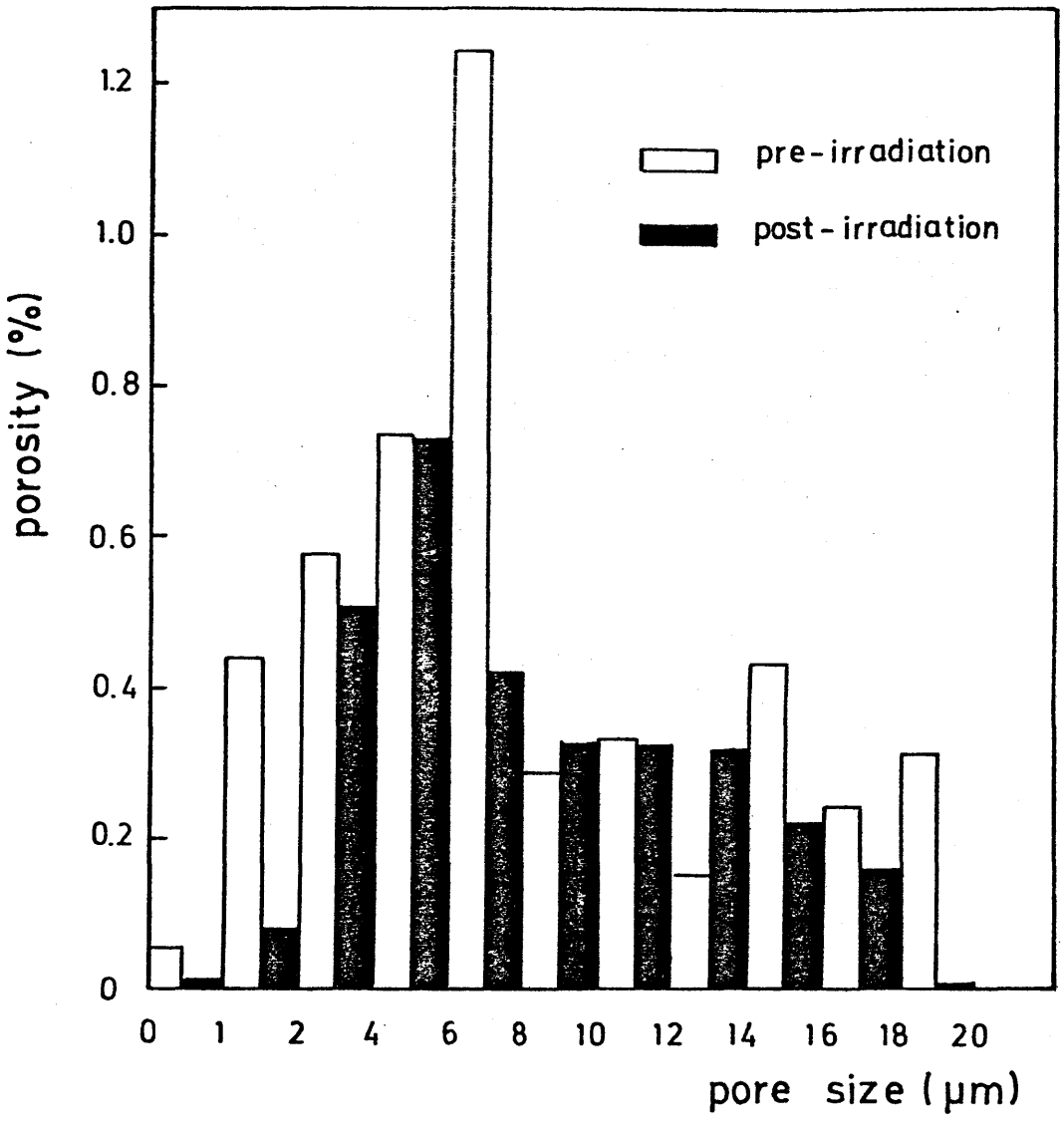

Fig.5-2. Pore size distribution of pre- and post-irradiation sample of 2.5 μm grain size.

5.3.2. Model for densification

Many models for the densification have been presented. Marlowe [21] proposed that irradiation induced diffusion controlled the densification to which the model for the thermal sintering of intermediate stage proposed by Coble [31-33] was applied. Carlson [22] proposed a mechanism that resolution of gas into fuel matrix resulted in the pore shrinkage. Other models were proposed by Stehle and Assmann [23,24] and MacEwen and Hastings [25]. Stehle and Assmann assumed that fission fragments passing close to the surface of a pore made many vacancies on the surface, and these vacancies migrated away from the pore. Thus the vacancies cause mass transfer of atoms to the pore, resulting in an eventual disappearance of the pores (see fig.5-3). MacEwen and Hastings proposed the model that pore shrinkage was caused by trapping of irradiation-produced point defects at sintering pores. Furthermore, Skinner et al. [18] and the Halden Reactor Projects [34] have introduced the empirical equations. Among the models, Marlowe's model is based on the assumption that the densification occurs by means of irradiation induced diffusion. The model, however, was based on only pore shrinkage. In addition, these authors considered that densification started at the beginning of reactor operation.

Our model is based on the fact that the density increase occurs after an initial bulk volume increase, which is the second

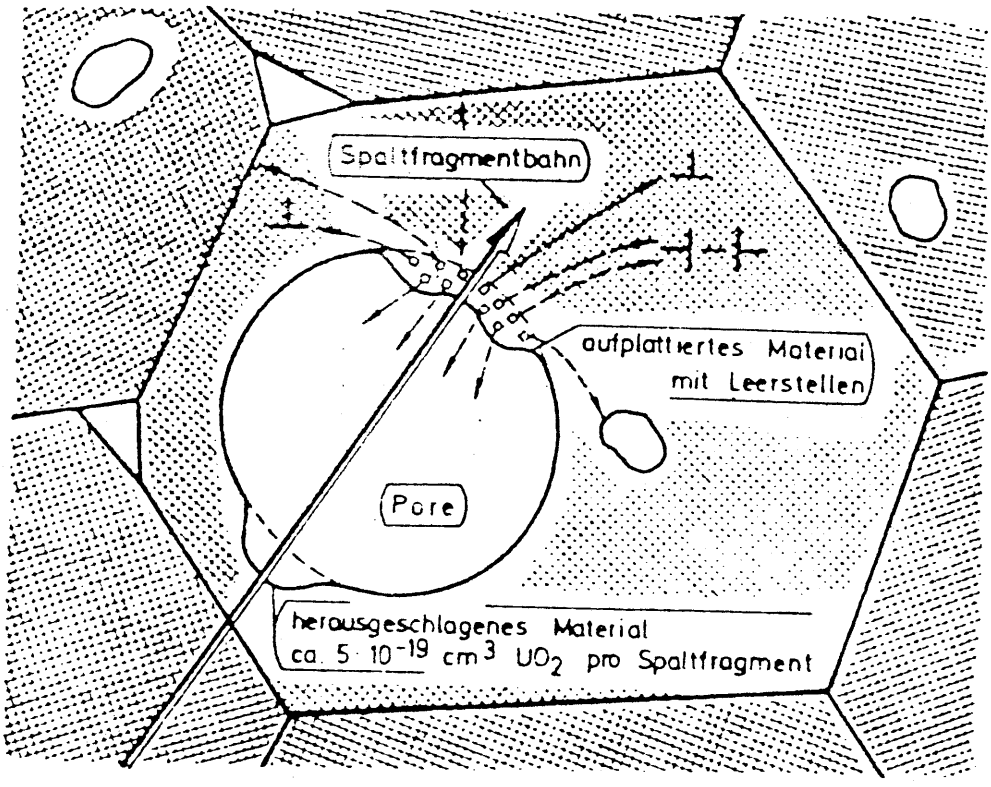

Fig.5-3. Model for the densification proposed by Stehle and Assmann [23].

stage of volume change described in Chapt. 2. Two mechanisms have been already considered for the density increase (volume decrease) in the chapter 2. The model, therefore, consists of two mechanisms, i.e., (1) annihilation of defects and defect clusters, and (2) pore shrinkage. In the annihilation mechanism, defect clusters which are less stable as mentioned in the chapter 2 decompose and form another type of defects, such as dislocation networks, and defects (i.e., interstitials) annihilate with vacancies in the third stage of lattice parameter change as mentioned in the chapter 1. While, in the pore shrinkage mechanism, lattice atoms migrate to pores by means of irradiation-induced diffusion, and it is due to both vacancy formation and migration. These phenomena are expected to occur under the circumstance that a large number of vacancies are produced.

The rate equation for the annihilation of defects has been already given in the chapter 1.

When the concentration of defect clusters which should have been annihilated at time t is defined as C_c, the rate of annihilation of defect clusters (dC_c/dt) depends on the concentration of the residual defects ($C_c^s - C_c$). Then, the following first order kinetic equation is adopted for the annihilation,

$$dC_c = k_c(C_c^s - C_c)dt, \qquad (5\text{-}1)$$

where k_c is a rate constant for annihilation of defect clusters

and C_c^S is the saturation value of C_c. By integrating eq.(5-1) with the boundary condition, $C_c = 0$ at $t = t_i$ (the density increase starts at t_i), the following equation is obtained,

$$C_c = C_c^S [1 - \exp\{-k_c(t - t_i)\}] . \qquad (5\text{-}2)$$

In the other case, suppose that the concentration of pores which have been sintered during irradiation at time t is C_s, the sintering rate of pores (dC_s/dt) depends on both the concentrations of vacancies (C_V) and of residual sintering pores ($C_s^S - C_s$). Then, we obtain the following equation,

$$dC_s = k_s(C_s^S - C_s)C_V dt, \qquad (5\text{-}3)$$

where k_s is a rate constant for sintering of pores and C_s^S is the saturation values of C_s. By integrating eq.(5-3) with the boundary condition, $C_s = 0$ at $t = t_i$ (it is assumed that dominant pore shrinkage starts at t_i), the following equation is given,

$$C_s = C_s^S [1 - \exp\{-k_s C_V(t - t_i)\}] . \qquad (5\text{-}4)$$

Both C_s and C_c correspond to the density increases due to pore shrinkage and annihilation of defect clusters (Δd_s and Δd_c, respectively) and both C_s^S and C_c^S to those at saturation (Δd_s^S and Δd_c^S).

The volume change due to the annihilation of defects corresponds to $3(\Delta a/a)$ in the third stage of lattice parameter change, and this is negligibly small as compared with those due to the annihilation of defect clusters, $\{(\Delta V_d/V) - (\Delta V_p/V)\} - 3(\Delta a/a)$, and pore shrinkage, $(\Delta V_p/V)$, (see fig.2-3 in the chapter 2). Therefore, the total density increase (Δd) is given as the sum of Δd_s and Δd_c neglecting the contribution of the annihilation of defects to the density increase as mentioned above, i.e.,

$$\Delta d = \Delta d_s + \Delta d_c$$

$$= (\Delta d_s^s + \Delta d_c^s) - \Delta d_s^s \exp\{-k_s C_V (t - t_i)\} - \Delta d_c^s \exp\{-k_c (t - t_i)\}. \qquad (5\text{-}5)$$

Eq.(5-5) is similar to an emprical equation obtained by the Halden Reactor Projects [34].

Δd_s corresponds to $\Delta V_p/V$ and Δd_c to the difference between $\Delta V_d/V$ and $\Delta V_p/V$. Δd_s^s and Δd_c^s are determined from the experimental results of $\Delta V_d/V$ and $\Delta V_p/V$ which have been shown in the chapter 2. The value of C_V has been already estimated in the chapter 4. The rate constants of k_s and k_c are calculated from the data of $\Delta V_d/V$ and $\Delta V_p/V$. The values of k_s, k_c, Δd_s^s, Δd_c^s and t_i are summarized in table 5-1. Comparison of the predicted values by eq.(5-5) using each value indicated in table 5-1

Table 5-1. Parameters k_s, k_c, Δd_s^s, Δd_c^s and t_i for the specimens of 5 and 2.5 μm grain sizes, respectively.

	$k_s(sec^{-1})$	$k_c(sec^{-1})$	$\Delta d_s^s(\%)$	$\Delta d_c^s(\%)$	t_i^*(hour)
5 μm	0.90×10^{-4}	1.33×10^{-6}	1.55	1.29	15.5
2.5 μm	1.09×10^{-4}	0.95×10^{-6}	1.80	2.18	13.7

*fission densities ($\dot{S} = \Sigma_f \phi_{th}$) are normalized to $\dot{S} = 10^{12}$ fissions/$cm^3 sec^{-1}$

with the experimental results is shown in fig.5-4. As shown in fig.5-4, the calculated curves by eq.(5-5) fit the data well except the results in JMTR. The deviations from the calculated curves are reasonably explained in terms of swelling due to fission products. The results in JMTR indicate that in-pile densification is saturated at about 1000 MWD/ton UO_2 and that at this dose the swelling due to fission products predominates on the volume change. The estimated swelling rate from this experimental results is in a range from 0.5 to 5 $\%(\Delta V/V)/10^{20}$ fissions/cm^3. These values are larger than those reported in literature (0.3 0.7 $\%(\Delta V/V)/10^{20}$ fissions/cm^3) [35], and the large swelling rate estimated above is probably due to the lower irradiation temperature than that obtained in the literature.

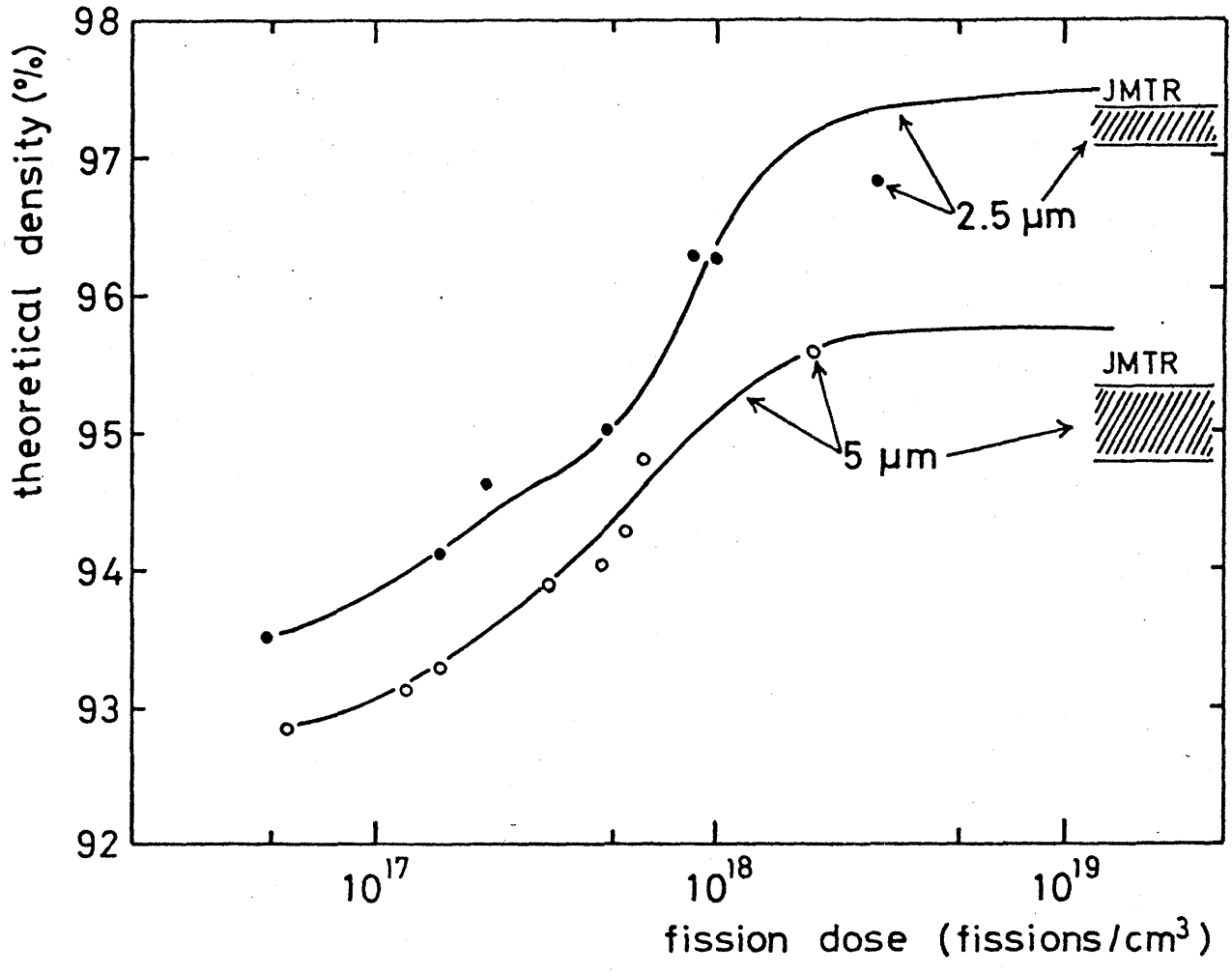

Fig.5-4. Comparison of the experimental data with the predicted values which are calculated by means of eq.(5-5). Hatchings represent the results of JMTR irradiation test.

References

[1] "Technical Report on Densification of Light Water Reactor Fuels", Regulatory Staff, U. S. Atomic Energy Commission, (1972).

[2] Letter from R. R. Koprowski of Rochester Gas and Electric Corporation to D. J. Skovholt of USAEC, dated June 22, 1972.

[3] Meno from R. H. Engelkeen to R. C. DeYoung, "Wisconsin Michigan Power Company (Point Beach 1), Docket No.50-266, Fuel Inspection Results", dated December 13, 1972.

[4] Memo from W. C. Seidle to H. D. Thornburg, "Carolina Power and Light Company (H. B. Robinson No.2), License No. DPR-23, Docket No.50-261", dated July 17, 1973.

[5] W. Chubb, A. C. Hott, B. M. Argall and G. R. Kilp, Nucl. Tech. 26 (1975) 486.

[6] D. H. Locke, Nucl. Tubes, (1972) 1015.

[7] I. J. Hastings, D. H. Rose and M. H. Schankula, J. Amer. Ceramic Soc. 58 (1974) 74.

[8] W. H. Culbert, Nucl. Safety, 14 (1973) 356.

[9] A. M. Ross, J. Nucl. Mater. 30 (1969) 134.

[10] J. A. Turnbull and R. M. Cornell, J. Nucl. Mater. 37 (1970) 355.

[11] W. Chubb, V. W. Storhok and D. L. Keller, J. Nucl. Mater. 44 (1972) 136.

[12] M. O. Marlowe, abstract in Amer. Ceramic Soc. Bull. 51 (1972) 388.

[13] M. C. J. Carlson, USAEC Report HEDL-TME-71-45, (1971).

[14] H. Assmann, H. Kroll and H. Roepenack, Report AED-CONF-71-100-27 (1971).

[15] W. R. Martin and J. R. Weir, USAEC Report ORNL-3103, (1961).

[16] H. M. Ferrari, E. Roberts and J. Scott, Paper 54, British Nuclear Energy Society Symposium on Nuclear Fuel Performance, London, UK (1973).

[17] D. Brucklacher and W. Dienst, ibid. Paper 60.

[18] J. Skinner, ibid. Paper 10.

[19] M. Uchida, K. Yanagisawa and M. Ichikawa, JAERI-M-6904 (1977).

[20] I. J. Hastings, AECL-4842 (1974).

[21] M. O. Marlowe, NEDO-12440 (1973).
Trans. Amer. Nucl. Soc., 17(1973) 166.

[22] M. C. J. Carlson, Nucl. Technol. 22 (1974) 335.

[23] H. Assmann and H. Stehle, REAKTORTAGUNG (1973) 409.

[24] H. Stehle and H. Assmann, J. Nucl. Mater. 52 (1974) 303.

[25] S. R. MacEwen and I. J. Hastings, Phil. Mag. 31 (1975) 135.

[26] R. S. Nelson, J. Nucl. Mater. 31 (1969) 153.

[27] M. O. Marlowe, J. Amer. Ceramic Soc. Bull. 51 (1972) 388.

[28] M. O. Marlowe, GEAP-12188, (1971).

[29] M. O. Marlowe, GEAP-12189, (1971).

[30] A. A. Solomon, J. L. Routbort and J. C. Voglewede, ANL-7857 (1971).

[31] R. L. Coble, J. Appl. Phys. 32 (1961) 787.

[32] R. L. Coble and T. K. Gupta, Intermediate Stage Sintering, in "Sintering and Related Phenomena", G. C. Kuczynski, N. A. Hooton and C. F. Gibbon (ed.), Gordon and Breach, New York, 1967.

[33] R. L. Coble, J. Appl. Phys. 32 (1961) 793.

[34] OECD Halden Reactor Project : 40th Ann. Report, (1972) p62.

[35] R. E. Skavdahl, et al., "International Symposium on Plutonium Fuels Technology, Arizona, Oct., 1967" Nuclear Metallurgy, 13, 457.

CONCLUSIONS

In this study, neutron irradiation effects on uranium dioxide (UO_2) were investigated. Main subject was the prediction of dose dependence of densification in oxide fuels. In order to understand this phenomena, the irradiation behavior of lattice defects such as interstitials and vacancies was investigated in connection with the results of lattice parameter and density measurements. Dose dependence of electrical properties which had not well understood was also investigated.

In Chapt. 1, the dose dependence of lattice parameter changes and their recovery annealing were studied and the results obtained were as follows:

(1) It was confirmed that three stages appeared in the course of lattice parameter and lattice strain changes and that the behavior of these changes depended on grain size. The dissociation of oxygen interstitial-vacancy complex which was proposed by Lee might be responsible for the reduction of lattice strain early in the first stage.

(2) The lattice expansion in the first stage completely recovered up to 500 ^{o}C, and two kinds of defects were involved in this stage. In the second stage more stable defects, which could not be recovered at 500 ^{o}C, were produced. In the third stage recovery of defects proceeded to some extent during irradiation, and therefore, the recovery of lattice expansion by thermal annealing of the specimen irradiated into this stage was less than that of the specimen

irradiated at the dose of around the end of the second stage.
(3) The effective volumes for lattice parameter change were calculated at each stage based on kinetic consideration of defects, and it was found that these volumes depended on grain size which was related to sink density.

In Chapt. 2, the dose dependence of volume changes was investigated based on the density measurement. The results were summarized as follows:
(1) There were four stages in the volume change, and the volume increased in the first and second stages and it decreased in the last two stages.
(2) The dose for the maximum volume increase ($\Delta V_d/V = 1.77$ %) corresponded to the reported dose of the maximum elongation of fuel pins in the starting period of previous BWR operation.
(3) The volume decrease (i.e., densification) occurred at the middle level of the second stage in the lattice parameter change. The porosity increase was also observed at the third and fourth stages of volume change. Therefore, two mechanisms (i.e., (i) the annihilation of defects and defect clusters and (ii) the pore shrinkage) were proposed for the density increase.

In Chapt. 3, the electrical properties such as electrical conductivity and thermoelectric power were measured after neutron irradiation, and the results obtained in this chapter were the followings:
(1) The initial decreases of conductivity and thermoelectric

power were explained in terms of both decomposition of oxygen interstitial-vacancy complexes and trapping of holes at primary defects. The decomposition of these complexes speculated already by lattice strain measurements described in the chapter 1 was confirmed to some extent.

(2) The thermoelectric power measurements indicated that the p-type conduction contributed to the electrical conductivity in UO_{2+x} irradiated up to 1.90×10^{18} fissions/cm^3. The abrupt increase in conductivity at higher dose (more than 1×10^{18} fissions/cm^3) was suggested to be due to the change of the conduction mechanism from the p-type extrinsic to intrinsic behavior.

In Chapt. 4, the concentrations of interstitials and vacancies during irradiation were estimated on the basis of the continuum model in crystals using the results of lattice parameter, density and porosity measurements. The result obtained especially for uranium vacancies was applied to the diffusional properties such as diffusion, creep and densification. The trend of the estimated creep rate corresponded to that of the experimental results of creep rate, and therefore, it was concluded that the concentration of uranium vacancies (C_{VU}^{irr}) and the irradiation-induced diffusion coefficient (D_U^{irr}) estimated in this chapter might be reasonable.

In the last chapter (Chapt. 5), the prediction of dose dependence of densification was investigated, and the kinetic equation which consisted of two exponential terms was proposed for it.

Two rate constants were calculated using the results of density and porosity measurements. At the last part of this chapter it was shown that the predicted curve by use of this equation fitted the experimental results well.

Observation of defects and defect clusters by means of electron microscope and more precise pore analysis must be needed in future, and furthermore, the measurement of irradiation-induced diffusion coefficients would remain.

ACKNOWLEDGEMENT

The author is grateful to Prof. Dr. Tomoo Kirihara, Nagoya University, for his continuiting guidance and encouragement through carrying out this study.

He wishes also to thank Dr. Hisayuki Matsui and Dr. Naomi Obata, Nagoya University, and Dr. Shoichi Nasu of Japan Atomic Energy Research Institute (JAERI) for their helpful discussions and suggestions.

The author would like to give his thank to Dr. Takeo Kikuchi of JAERI for carrying out this study which was joint research between Kirihara laboratory in Nagoya University and his laboratory in JAERI (Fuel Property Laboratory).

He would like to express appreciation to Mrs. Osamu Nakagawa (JRR), Michio Shimizu, Takashi Iwai and Mamoru Tomita (JMTR) of JAERI, and Mr. Minoru Narui, Tohoku University.

The author is also indebted to the members of Kirihara laboratory, especially to Mrs. Toshihisa Koike, Akio Harada, Osamu Takagi, Yutaka Iwata and Mikio Horiki for their assistances in the experimental work.

He would like to thank to Dr. Hj. Matzke, EURATOM, Karlsruhe, for his fruitful discussions and interests to this work.

LIST OF PUBLICATIONS

(1) Tomoo KIRIHARA, Nobuo NAKAE, Hisayuki MATSUI, Masayoshi TAMAKI Shoichi NASU and Takeo KIKUCHI,
"FISSION DOCE DEPENDENCE OF THE LATTICE PARAMETER CHANGE IN FUEL ELEMENTS"
Proc. Int. Conf. Plutonium 1975 and other actinides, North Holland Publ. Co., Amsterdam (1976) p.903

(2) Nobuo NAKAE, Akio HARADA, Tomoo KIRIHARA and Shoichi NASU,
"IRRADIATION INDUCED LATTICE DEFECTS IN UO_2"
J. Nucl. Mater. (1978) 71, 314 ~~in print~~

(3) Nobuo NAKAE, Toshihisa KOIKE and Tomoo KIRIHARA,
"ELECTRICAL CONDUCTIVITY AND THERMOELECTRIC POWER IN IRRADIATED UO_{2+x}"
J. Nucl. Mater. (1978) in print

(4) Nobuo NAKAE, Tomoo KIRIHARA and Shoichi NASU,
"IRRADIATION INDUCED VOLUME CHANGE IN UO_2"
J. Nucl. Mater. (1978) in print